Correlating gas permeability and rigidity during the physical aging of polymers of intrinsic microporosity using atomic force microscopy

Mariagiulia Longo[†], Maria Penelope De Santo[‡], Elisa Esposito[†], Alessio Fuoco[†], Marcello Monteleone[†], Lidietta Giorno[†], Bibiana Comesaña-Gándara[§], Jie Chen[§], C. Grazia Bezzu[§,//], Mariolino Carta[#], Ian Rose[§], Neil B. McKeown[§,], Johannes C. Jansen[†,*]*

[†]Institute on Membrane Technology, CNR-ITM. Via P. Bucci 17/C, 87036 Rende (CS), Italy.

[‡]Department of Physics and CNR-Nanotec, University of Calabria, Rende (CS), Italy.

[§]EaStCHEM, School of Chemistry, University of Edinburgh, David Brewster Road, Edinburgh, EH9 3FJ, (UK).

[#]Department of Chemistry, Swansea University, College of Science, Grove Building, Singleton Park, Swansea, SA2 8PP, (UK).

KEYWORDS: Atomic force microscopy; Force spectroscopy; Mechanical properties; Gas separation membranes; PIMs, Physical aging.

ABSTRACT: The relationship, during physical aging, between the transport properties and Young's modulus for films of polymers of intrinsic microporosity (PIM) was investigated using pure gas permeability and atomic force microscopy (AFM) in force spectroscopy mode. Excellent agreement of Young's modulus measured for the archetypal PIM-1 with values obtained by other techniques in the literature, confirms the suitability of AFM force spectroscopy for the rapid and convenient assessment of mechanical properties. Results from different polymers including PIM-1 and five ultrapermeable benzotriptycene-based PIMs provide direct evidence that size selectivity is strongly correlated to Young's modulus. In addition, film samples of one representative PIM (PIM-DTFM-BTrip) were subjected to both normal physical aging and to accelerated aging by thermal conditioning under vacuum for comparison. Accelerated aging resulted in a similar decrease in permeability and increase in Young's modulus as normal aging, however, significant differences suggest that thermally induced accelerated ageing occurs throughout the bulk of the polymer film whereas normal aging occurs predominantly at the surface of the film. For all PIMs, the increased in film rigidity upon aging led to an increase in gas size selectivity.

1 Introduction

The separation and purification of large quantities of chemical products account for 10-15% of the world's energy consumption, with the treatment of gas and vapor mixtures being the central process of many industrial applications.[1] The development of membrane technology plays an important role in several large-scale gas separation applications, including CO_2 capture, natural gas treatment and biogas upgrading.[2,3] The key to boost the use of membrane technology in these large-scale applications is the development of novel performing materials with improved

permeability (productivity) and selectivity (purity of the products).[4] However, polymeric materials for gas separation suffer from a trade-off between these two quantities, which is well-represented by the Robeson Upper Bounds.[5,6] In a theoretical analysis, Freeman *et al.* suggested that improvements in the performance of gas separation membranes require the synthesis of novel polymers with a simultaneous increase of chain stiffness and interchain separation.[7] This design strategy was consistent with the structure of the first Polymer of Intrinsic Microporosity (PIM-1) in 2004,[8] and led to successive modifications, including those containing rigid bridged bicyclic units such as Tröger's base.[9] PIMs demonstrate attractive properties for membranes with a combination of very high permeability, good separation factor, good mechanical properties and capability to be solution-processed.[10] Very recently, rigid amidoxime-modified PIMs achieved highly permeable, selective and plasticization-resistant membranes for natural gas sweetening.[11]

Like all glassy polymers with high fractional free volume, PIMs suffer from physical aging as a consequence of the non-equilibrium nature of the glassy state, leading to a slow relaxation and rearrangement of the molecular structure.[12] Aging strongly depends on the previous processing and thermal history of the samples,[13] and widely different treatments are reported in the literature to condition samples before the analysis, which may therefore lead to significant differences in the test results. Permeability measurements are either performed on freshly prepared samples, after alcohol treatment, or after drying under vacuum at elevated temperatures.[14,15] Drying conditions vary from 12 h at 70 °C under vacuum,[16] 24 h at 120 °C under vacuum with additional 2 weeks of aging,[17] 4h at 140 °C under vacuum,[18] or 125 °C overnight in air.[19] On the other hand, for the measurement of the BET surface area, which is often correlated with the transport properties, powder samples are usually degassed at 120 °C for 16 h[20,21] or at 150 °C for 12 h[22] under high vacuum. It has been noted that drying at elevated temperatures causes accelerated aging, so that a

lower permeability state is reached immediately, but with a slower further decrease during subsequent aging.[18] Prolonged aging of thick films has a considerable effect on the transport properties and can be used to mimic the rapid aging in thin dense selective layer of composite or asymmetric membranes for gas separation.[23] For conventional polymers, Paul *et al.* found that physical aging is much faster in thin films and they ascribed this to the diffusion of free volume elements to the surface.[24–26] This surface related mechanism appears relevant for PIM-1 as indicated by depth-resolved PALS measurements.[27]

Gas permeation measurements are a very powerful technique to track the aging of membranes.[24] Aging leads to a decrease in permeability and for many glassy polymers a concurrent increase in selectivity, generally proceeds in a manner nearly parallel to the upper bound lines.[28] Moreover, Rose *et al.* discussed that there may exist a relationship between the transport properties and the mechanical properties in PIMs.[29] Therefore, a study of PIM aging, to seek greater understanding of the relationship between gas separation performance and mechanical properties on a time scale that is close enough to the normal life time of a membrane is desirable. The few reports on the mechanical properties of PIMs,[30–35] using different techniques, reveal that the elastic modulus of PIMs are in the range that is typical of glassy polymers.[29,36] However, common tensile tests require multiple specimens of a relatively large sample size, and to the best of our knowledge a systematic analysis of the effect of physical aging on the mechanical properties of PIMs has never been performed. For situations where only a small amount of sample is available, a versatile and widely used alternative is force spectroscopy. In this technique, an atomic force microscope (AFM) tip scans over an area of the sample surface, and the corresponding applied force versus tip displacement (FD curve) is determined.[37,38] FD measurements are macroscopically non-destructive, require millimeter-sized samples and, thus, could potentially allow a large number of

tests to be performed even on relatively exotic PIMs where only small samples are available. Polak-Kraśna *et al*. used AFM nanoindentation analysis to determine the elastic moduli of PIM-1 films at different indentation depths,[33] obtaining results that are in good agreement with data acquired with tensile tests and DMTA.[32] Song *et al*. performed nanoindentation on PIM-1 to study the effect of thermal-oxidative treatment on the polymer stiffness.[35] Comparative studies have demonstrated that results obtained by AFM force spectroscopy are fully consistent with those obtained by tensile tests for neat polymers and more complex systems such as mixed matrix membranes.[39,40]

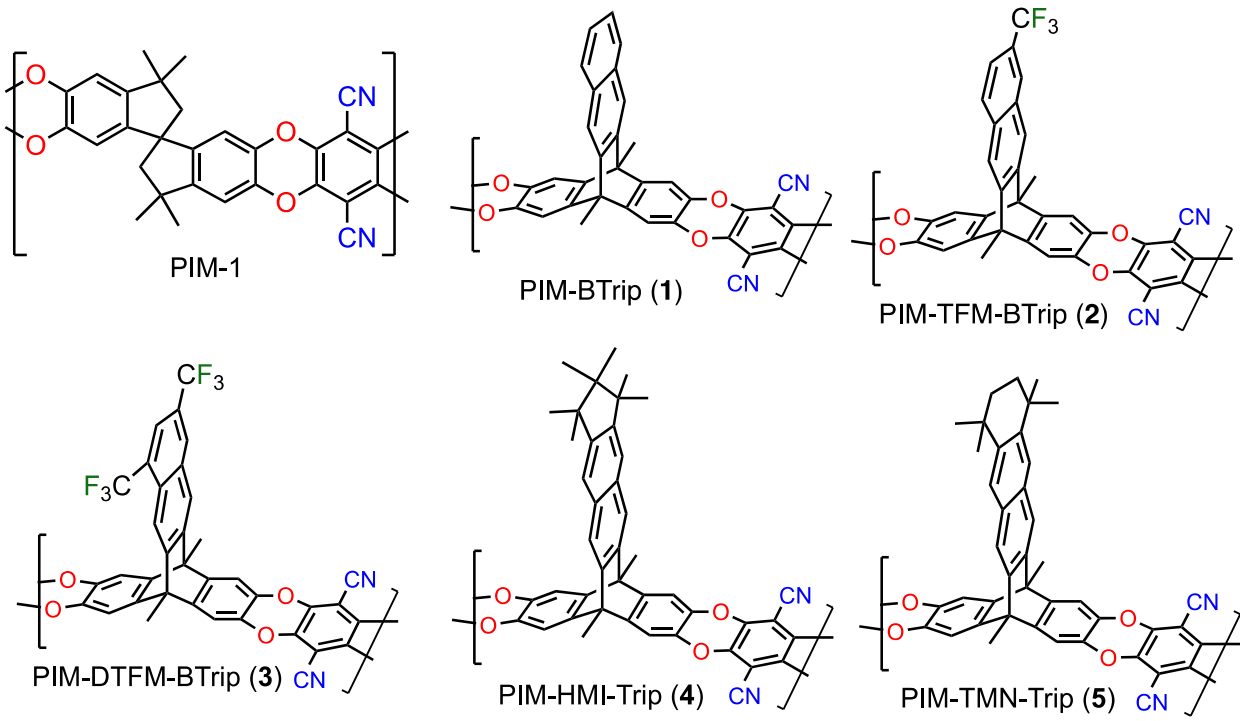

Figure 1. Structure of PIM-1 and the ultrapermeable PIMs used in the present work.

Here, we investigate the correlation of the mechanical and gas transport properties via a systematic study of five highly permeable PIMs (Figure 1), including a more detailed analysis of PIM-DTFM-BTrip as a function of the sample history (i.e. the effect of physical aging accelerated by thermal treatments relative to that at ambient conditions). PIM-1 is used as a reference polymer

to allow comparison with mechanical properties already reported in the literature. The aim of this study is to provide new insight into the origin of the strong size-selectivity of PIMs, and of the transport properties in general. This study is of great practical interest because knowledge of the correlation between polymer structure, physical aging, mechanical and transport properties may provide a key to the development of polymers for even more efficient gas separation membranes.

2 Experimental part

2.1 Membrane preparation and conditioning

Polymers of intrinsic microporosity, archetypal PIM-1[8,33], and ultrapermeable PIM-BTrip (**1**), PIM-TFM-BTrip (**2**), PIM-DTFM-BTrip (**3**), PIM-HMI-Trip (**4**) and PIM-TMN-Trip (**5**) (Figure 1) were synthesized and the membranes were prepared in the form of dense self-standing films as described previously.[41] As a post-treatment step, all membranes were soaked in methanol for 24h and dried for one day at ambient conditions, loosely pressed between two porous glass disks to maintain a flat shape and to allow the methanol removal via evaporation. This treatment resets the thermodynamic polymer history[27] and removes traces of residual solvent after membrane preparation.[17,42,43] The casting solvent, membrane treatment and the film thickness are reported in Table 1. The films were thick enough and were MeOH treated to guarantee that the transport properties were neither thickness-dependent, nor dependent on the casting solvent. Methanol was provided by VWR chemical and used without further purification.

An additional membrane of PIM-DTFM-BTrip was split into four completely equivalent sample specimens and all four were soaked in methanol and dried in air as above. Two of these were then further conditioned under vacuum at 140 °C in an attempt to accelerate the aging process. Of the samples treated only in methanol and those thermally conditioned, one specimen was tested

immediately and the other was aged for 30 days at ambient conditions before the first measurement. The codes of PIM-DTFM-BTrip membranes and the different treatments are reported in Table 1.

Table 1. Membrane code, pre-measurement history, and thickness of the films studied in the present work.

Polymer	Casting solvent	Membrane code and history [a)]	Thickness (μm)	Ref.
PIM-1	Chloroform	MeOH [b)]	88	This work
		+140°C_4h	85	This work
		MeOH+aged 2219d [b)]	91	This work
PIM-BTrip	Quinoline	MeOH	160	Ref [41]
PIM-TFM-BTrip	Quinoline	MeOH	176	Ref [41]
PIM-DTFM-BTrip	Quinoline	MeOH	106	This work
		+140°C_4h	149	This work
		MeOH_30d	156	This work
		+140°C_4h_30d	186	This work
PIM-HMI-Trip	Chloroform	MeOH	135	Ref [41]
PIM-TMN-Trip	Chloroform	MeOH	166	Ref [41]

[a)] Membrane codes representing their preparation history:

MeOH: Membrane soaked in methanol, dried in air for 24 h, and tested immediately.

MeOH_30d: Membrane soaked in methanol, dried in air for 24 h, and stored for 30 days before testing.

+140°C_4h: Membrane soaked in methanol, dried in air for 24 h, heated at 140 °C for 4 h, and tested immediately.

+140°C_4h_30d: Membrane soaked in methanol, dried in air for 24 h, heated at 140 °C for 4 h, and stored for 30 days before testing.

MeOH+aged 2219d: Membrane soaked in methanol, dried in air for 24 h, and aged for 2219 days before testing.

[b)] Different samples

2.2 Force spectroscopy

Measurements of the elastic modulus were performed at room temperature in air on a Multimode 8 AFM system with a Nanoscope V controller, as described elsewhere,[39] with the only difference that the measurements were performed in air and not in liquid. Cantilevers of the type CP-PNP-SiO (SQUBE), with a spherical tip and a nominal radius of 2 µm (± 5%), were used. The cantilevers were individually calibrated using the appropriate calibration probes (CLFC, Force calibration cantilevers, Bruker), in accordance with the instructions of the producer.[44] The calibrated elastic constants were in the range of 32.5 N m^{-1} to 46.6 N m^{-1}. The local elastic modulus was obtained by quantitative analysis of the Force-Deformation (FD) curve via modelling of the contact region with the general theory of contact mechanics.[45] The force and penetration depth were optimized in order to avoid involuntary damage of the sample by the tip.[37] The elastic modulus, *E*, was calculated by fitting the single curve with the Hertz model,[46] which predicts that the force increases non-linearly with the indentation depth, δ:[47]

$$F = \frac{4}{3}\frac{E\sqrt{r\,\delta^3}}{(1-\upsilon^2)} \qquad (1)$$

where *F* is the loading force, *r* is the tip's radius of curvature. The parameter υ is Poisson's ratio, which compares the strains in the transverse and longitudinal directions under uniaxial stress and is assumed to be 0.3 in the case of glassy polymers.[48] For each membrane, 60 FD curves were

recorded after the permeation tests, on three different areas and at a scan rate of about 400 nm s^{-1}. Data were fitted using the NanoScope Analysis 1.5 software and the results were statistically analyzed using Microsoft Excel.

2.3 Gas permeation analysis

Permeation tests were carried out with single gasses at 25 °C and at a feed pressure of 1 bar, using a fixed volume/pressure increase apparatus (Elektro & Elektronik Service Reuter, Geesthacht, Germany), as described previously.[49,50] All gases were supplied by Sapio (Italy) at a minimum purity of >99.9995%. The gases were tested in the order H_2, He, O_2, N_2, CH_4, CO_2, O_2 and N_2. The tests of O_2 and N_2 were repeated to confirm that there were no substantial changes in performance after CO_2, thus excluding swelling and dilation phenomena. The permeability, *P*, is calculated from the slope of the time-pressure curve in pseudo-steady state condition given by:[51]

$$p_t = p_0 + \left(\frac{dp}{dt}\right)_0 \cdot t + \frac{RT \cdot A}{V_P \cdot V_m} \cdot \frac{p_f \cdot P}{l} \cdot \left(t - \frac{l^2}{6D}\right) \qquad (2)$$

in which p_t is the permeate pressure at time *t*, p_0 is the starting pressure, $(d_p/d_t)_0$ is the baseline slope, *R* is the universal gas constant, *T* is the absolute temperature, *A* is the effective membrane area, V_P is the permeate volume, V_m is the molar volume of the permeating gas at standard temperature and pressure (0 °C and 1 atm), p_f is the feed pressure, and *l* is the membrane thickness. The baseline slope and the starting pressure are normally negligible if the membrane is sufficiently degassed and defect-free. The diffusion coefficient, *D,* was determined from the time-lag according to the equation:

$$D = \frac{l^2}{6\Theta} \qquad (3)$$

where Θ is the so-called diffusion time-lag. Assuming the solution-diffusion mechanism, the gas solubility coefficient, *S*, is calculated indirectly as the ratio of the permeability over the diffusion coefficient:

$$S = \frac{P}{D} \qquad (4)$$

3 Results and discussion

3.1 PIM-1 reference material

The 3D histogram in Figure 2a shows the frequency distribution for *ca.* 60 individual measurements of Young's modulus of a PIM-1 film soaked in methanol and then thermally treated or aged. Repeated measurements at different points of the sample result in a narrow distribution of Young's modulus around the average value. The value of the fresh sample (dark blue) is in good agreement with the data available in the literature from different techniques (1 - 1.7 GPa)[32,35,52,53] and confirms the validity of the AFM force spectroscopy method. The average value depends strongly on the sample history, as can be seen from the modulus of the film that was thermally conditioned after soaking in methanol (red), which shifts from 1.25 ± 0.03 GPa to 1.66 ± 0.05 GPa. The modulus of the membrane that was soaked in methanol and then aged for 2219 days under ambient conditions (light blue) further increases to 2.03 ± 0.05 GPa. Figure 2b shows the correlation between permeability and Young's modulus of PIM-1. The permeability decreases with increasing Young's modulus independently of the sample history (accelerated thermal aging or natural aging), and this trend is mostly due to a decrease in the diffusion coefficient (Figure S1a). Instead, solubility is virtually unaffected (Figure S1b).

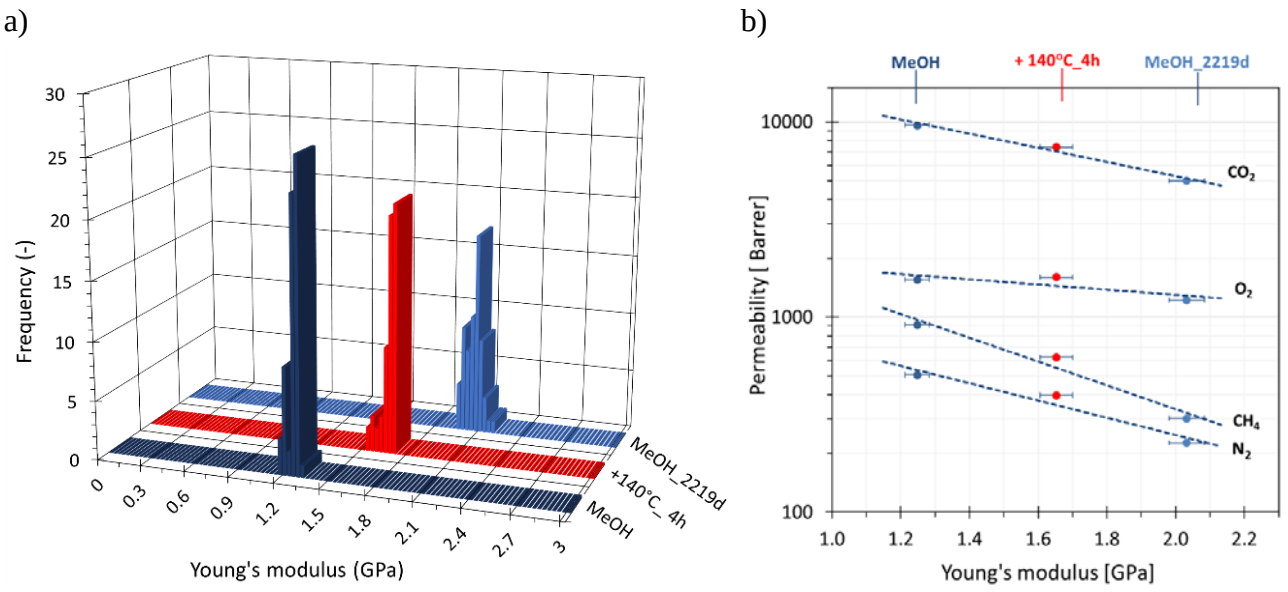

Figure 2. (a) Frequency distribution of Young's modulus of a PIM-1 sample after MeOH treatment (dark blue) and subsequent thermal conditioning at 140 °C under vacuum (red) or after 2219 days of aging from the MeOH treatment (light blue). (b) Correlation of the permeability coefficient of O_2, N_2, CH_4 and CO_2 with Young's modulus of the samples. The symbol and the horizontal error bar show the average modulus and the standard deviation of Young's modulus, respectively, calculated from the 60 individual measurements represented in the frequency distributions. The dashed lines are indicated as a guide to the eyes.

3.2 Ultrapermeable PIMs

Figure 3a shows the frequency distribution of Young's moduli for five ultrapermeable PIMs after methanol soaking and drying overnight. Figure 3b shows the same samples, with the exception of PIM-BTrip, after 60 days of aging. Aged PIM-BTrip films proved unsuitable for measurement due to the formation of shallow surface cracks with similar dimensions as that of the

AFM tip (Figure S2 and Figure S3). In all cases, the modulus increases for the 60 days aged films at much higher values than those of 2219 days aged PIM-1. This suggests that in the state with the highest excess free volume, just after MeOH treatment, the polymer has a relatively soft structure, and the aging leads to a denser packing arrangement with an increase in the bulk stiffness of the materials, along with a decrease in permeability.

For all gases, the permeability tends to decrease with increasing Young's modulus (Figure 3c) in a roughly exponential fashion, with only PIM-HMI-Trip falling slightly below the trend. This correlation is interesting in view of Freeman's analysis of the Robeson Upper bound relationship,[7] and in view of the studies claiming that for instance TR polymers owe their molecular sieve-like size selectivity to the increased rigidity of the polymer after the thermal rearrangement.[54] The decreasing permeability upon aging is usually strongest for the larger gas species and this is correlated with increased size-selectivity.[55] Similarly, diffusivity decreases with Young's modulus in a similar fashion when a sufficiently wide range of modulus values is covered but with some deviations from the trend line for the individual polymers (Figure 3d), suggesting that the correlation between diffusivity and Young's Modulus is not as strong as that between permeability and Young's Modulus. The deviation from the trend line most likely occurs because sample modulus is not the only factor determining the size selectivity, but also the total free volume and its size distribution. Depending on the gas type and sample history, the standard deviation in the permeability is always below 18%, but typically it is in the range of the symbol size in the graphs,[41] and therefore it does not affect the observed trends or the conclusions of the manuscript.

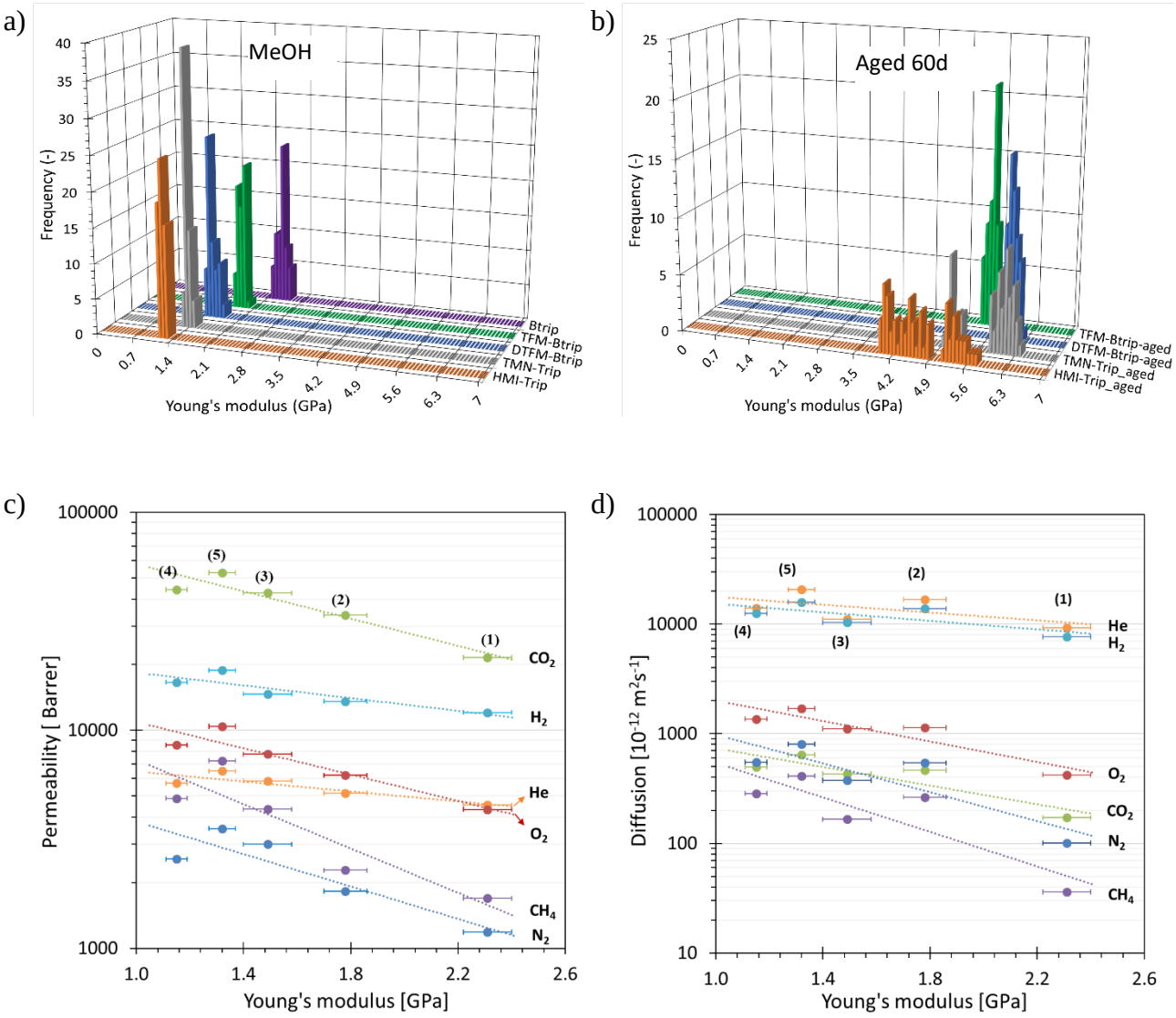

Figure 3. Frequency distribution of Young's modulus of the fresh ultrapermeable PIM-BTrip (**1**), PIM-TFM-BTrip (**2**), PIM-DTFM-BTrip (**3**), PIM-HMI-Trip (**4**) and PIM-TMN-Trip (**5**) samples tested after methanol treatment and dried in air for 24 h (a) and of the same samples after 60 days of aging (b). Plot of the correlation of the permeability coefficient[41] (c) and of the diffusion coefficients (d) with Young's modulus of the polymers. The symbol and the horizontal error bar (shown only in the CO_2 series for clarity) show the average value and the standard deviation of Young's modulus,

respectively, calculated from the 60 individual measurements represented in the frequency distributions. The dotted lines serve as a guide to the eye.

3.3 Effect of aging and conditioning of the sample on gas transport

Figure 4 shows the permeability and the diffusion coefficient with their related selectivities for a series of gases upon aging of a MeOH treated sample and of a sample evacuated for 4h at 140 °C. The permeability gradually decreases as a function of aging time for all gases in both films, with lower values for the thermally conditioned sample due to the accelerated physical aging (Figure 4a). He and H_2 (not shown), follow the same qualitative trends in permeability as O_2, N_2, CH_4 and CO_2, but their time lag is too short to measure the diffusion coefficient accurately. The decrease in permeability is associated with a weak increase in selectivity (Figure 4b), following the same trend previously described for physical aging of other PIMs and glassy polymers.[18,24] This trend is clearer on the Robeson plots (Figure 5). Diffusivity follows the same trend as permeability (Figure 4c), whereas the solubility is hardly affected by either aging or thermal treatment of the samples (Figure 4d). Thus, aging affects the mobility of the polymer chains, their packing density and the overall free volume without substantial changes in the affinity for the gas. For both samples, the diffusion coefficients decrease in the order $O_2 > CO_2 > N_2 > CH_4$, according to their effective gas diameters.[56] This is typical for nearly all dense membranes for which transport is governed by the solution-diffusion transport mechanism, and the effect is particularly strong for PIMs, known for their strong size-selective character.[55,57]

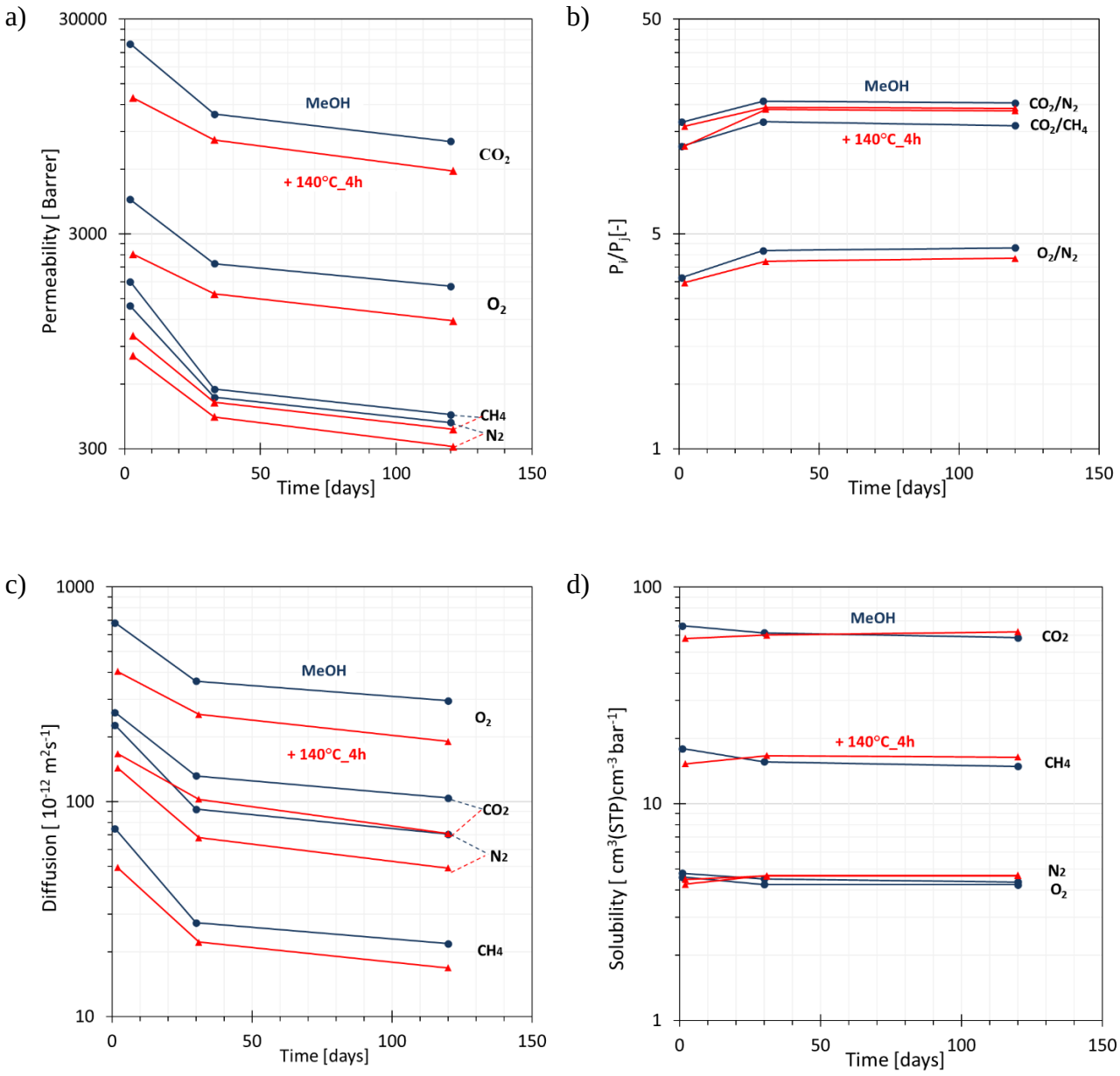

Figure 4. Transport properties of O_2, N_2, CH_4 and CO_2 upon aging of the PIM-DTFM-BTrip (**3**) membranes after methanol soaking (•) and after methanol soaking and thermal conditioning at 140 °C for 4 h (▲): (a) permeability, (b) permselectivity (c) diffusivity and (d) solubility. (Note that the dotted lines link the curves with the gas name., 1 Barrer = 10^{-10} cm^3 (STP) cm cm^{-2} s^{-1} $cmHg^{-1}$).

Interestingly, aging seems to be triggered by the permeability measurement itself, because the samples tested 30 days after the MeOH treatment, with or without conditioning at 140 °C, show the same *P* and *D* as the samples immediately tested, and much higher *P* and *D* than the samples that were tested and then aged for 30 days (Figure S5). This suggests that residual methanol reduces aging until it is removed by the vacuum applied on the membrane before the permeability tests. However, it has been noted previously that repetitive exposure to MeOH vapor cannot completely suppress physical aging.[19]

The Robeson plots of PIM-DTFM-BTrip for the four relevant gas pairs CO_2/CH_4, CO_2/N_2, O_2/N_2, and He/N_2 (Figure 5a-d) show that aging generally leads to a decrease in the permeability and an increase in selectivity, more or less parallel to the Robeson upper bound,[28] as recently observed for all members of the benzotriptycene-based PIM family.[41] The strong increase in He/N_2 selectivity (Figure 5d), evidences a distinct size-sieving ability of the polymer, which further increases upon aging. Instead, the thermal treatment at 140 °C accelerates aging and reduces the permeability of the samples, but without the desired increase in selectivity. This makes thermal treatment less attractive to optimize performance.

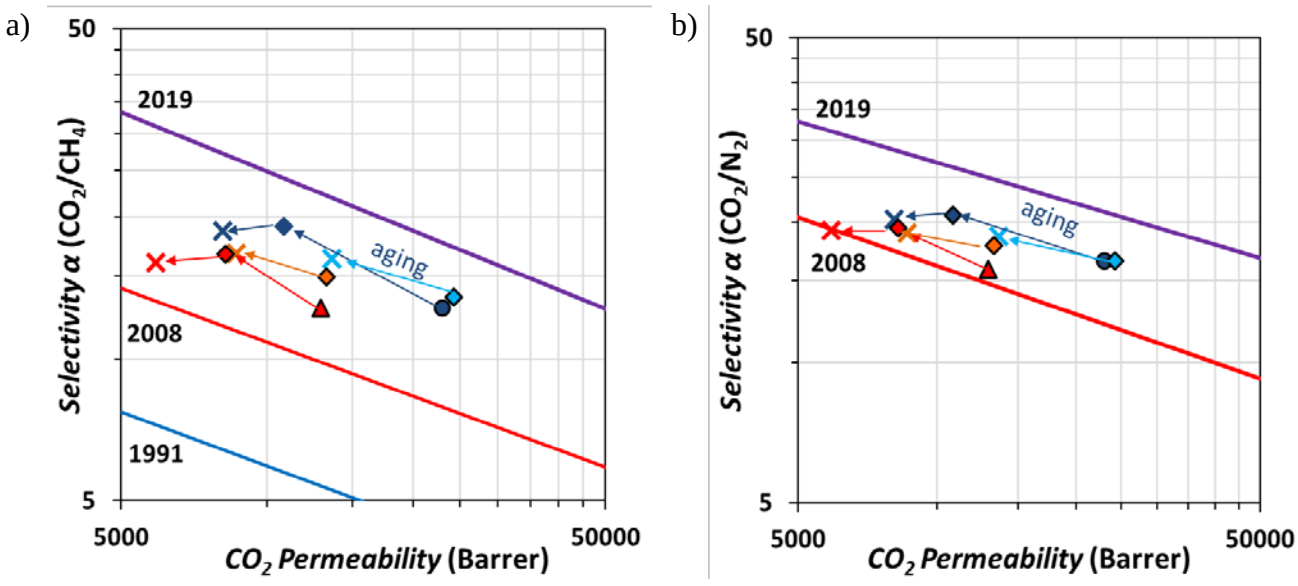

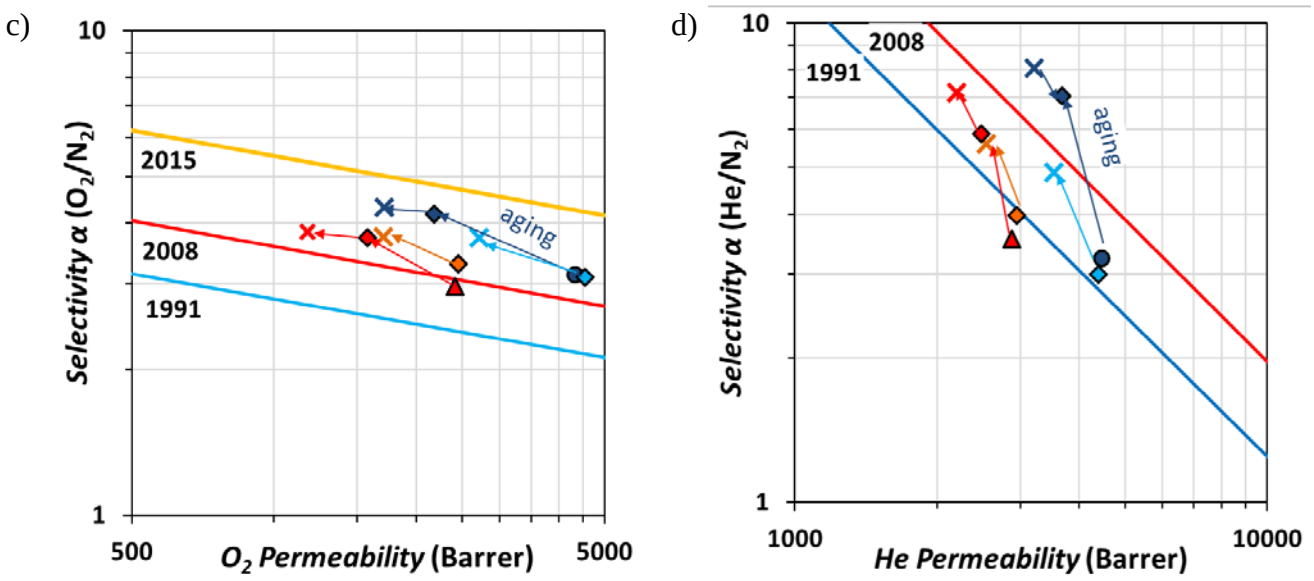

Figure 5. Robeson plots of PIM-DTFM-BTrip (**3**) for CO_2/CH_4 (a), CO_2/N_2 (b), O_2/N_2 (c), and He/N_2 (d) with the 1991 upper bounds indicated by a blue line, 2008 by a red line and those proposed for 2015 by yellow lines. Blue symbols show the data for the sample MeOH (•) and subsequently aged (30d (♦), 120d (✕)). Light blue symbols show the data for the sample MeOH_30d and subsequently aged (30d (♦), 120d (✕)). Red symbols show the data for the sample 140 °C_4h (▲), and subsequent aging (30d (♦), 120d (✕)). Orange symbols show the data for the sample 140°C_4h_30d and subsequent aging (30d (♦), 120d (✕)).

3.4 Effect of physical aging on the mechanical properties

The sample history of PIM-DTFM-BTrip also strongly affects its mechanical properties, as witnessed by a significant increase of Young's modulus after conditioning under different conditions. Figure 6 shows the frequency distribution of Young's modulus of the membrane only soaked in methanol (a), and the one further thermally conditioned (b). The three distributions for each sample represent the fresh, the 33 days aged, and the 120 days aged sample, respectively,

with the brightest color for the longest aging. In all cases, the average Young's modulus increases with aging time. Normal aging occurs predominantly at the surface of the film due to the enhanced mobility near the surface or to the diffusion of free volume toward the surface of the film, allowing the polymer at the surface or in thin films to reach a lower free volume state more quickly than bulk samples,[13,26] and creating a concentration gradient of fractional free volume near the surface.[27,58] The thermal conditioning of the membrane leads to a higher initial modulus but slower further increase over time, consistent with the thermal treatment initially accelerating aging and stabilizing the mechanical properties. This suggests that thermally induced accelerated ageing occurs throughout the bulk of the polymer film, as a trade-off between increased thermal motion at elevated temperature and increased free volume due to thermal expansion. Remarkably, for both the fresh MeOH treated sample and the heat-treated sample, the permeability (Figure S5) and Young's modulus (Figure S6) change much less upon storage of the samples for 30 days without prior testing, than it does upon aging for 30 days after immediate testing. This suggests that the alternating vacuum and permeation of the samples actually triggers or accelerates the aging process.

a)

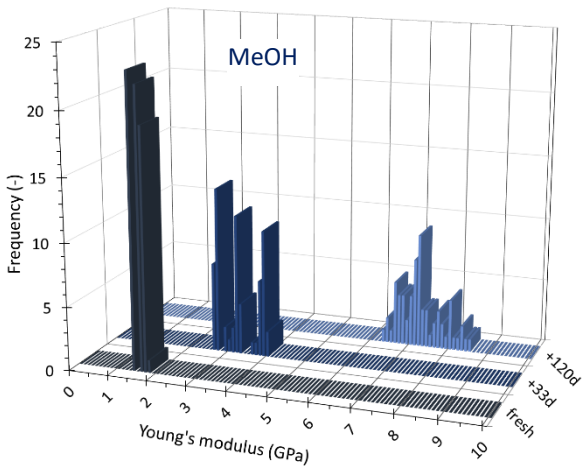

b)

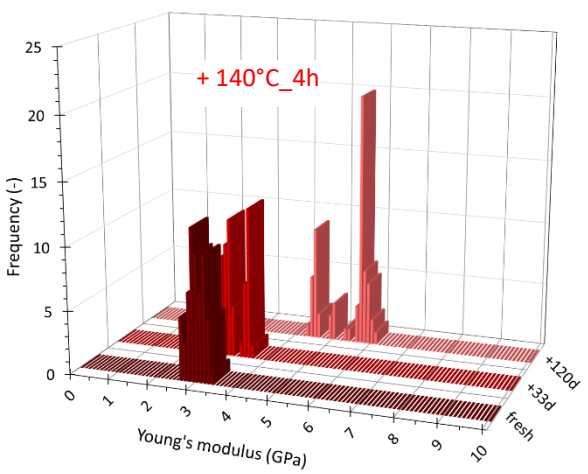

Figure 6. Effect of physical aging and post treatments on Young's modulus of PIM-DTFM-BTrip (**3**) films after MeOH treatment (a) and after conditioning at 140 °C (b). The three groups in the charts represent the frequency distribution of the samples after different aging time.

3.5 Correlation between gas transport and polymer film rigidity

Figure 7 shows the correlation of the gas transport parameters with Young's modulus of the methanol treated samples of the benzotriptycene PIMs. The permeability decreases with increasing Young's modulus (a) and this is due to a decrease in the diffusion coefficient (Figure 7 b), consistent with the behavior observed for PIM-1. Solubility is not correlated with the mechanical properties and remains virtually constant (Figure S7). The correlation between permeability and Young's modulus is not limited to the MeOH treated sample but it is common for all samples with different histories (Figure S8). The observed correlation shows a general trend, almost independent of the specific sample history (Figure S9).

a) b)

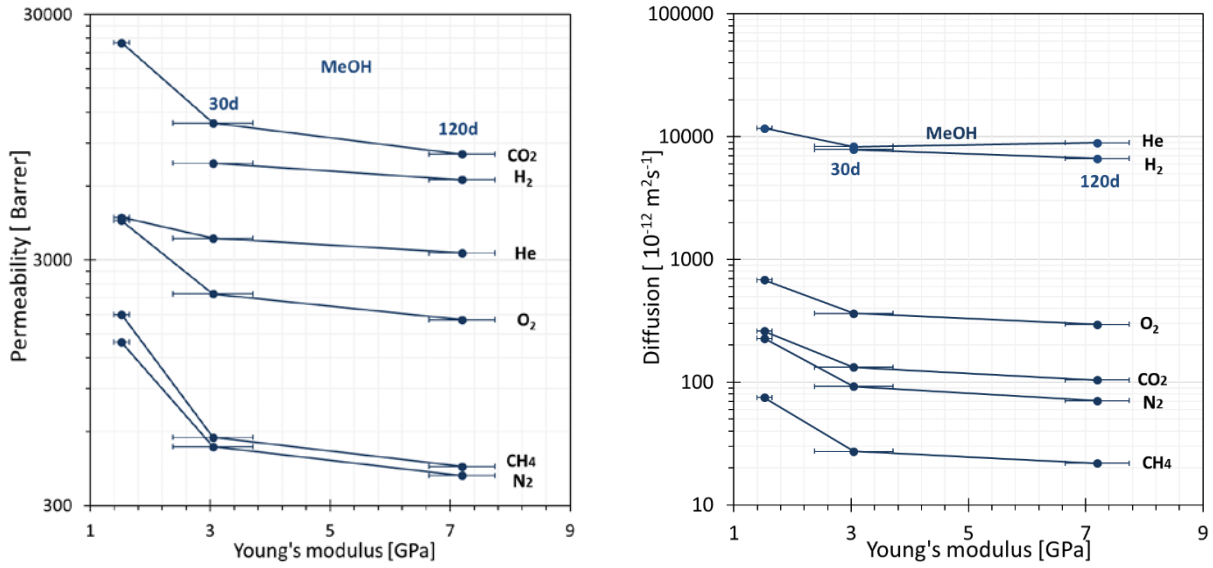

Figure 7. Correlation between Young's modulus and permeability (a) or diffusion coefficient (b) for O_2, N_2, He, H_2, CH_4 and CO_2 in the freshly prepared samples of PIM-DTFM-BTrip (**3**) after MeOH. The symbol and the horizontal error bar represent the average modulus and the standard deviation, respectively, calculated from the 60 individual measurements.

The stiffening of the samples on aging hinders the diffusion of the penetrants, particularly the larger gas molecules, though the membrane. At the same time, the decreased chain mobility leads to an increase in the energetic selectivity, increasing the size-sieving properties of the materials, and then the overall selectivity, consistent with a previous study on temperature dependent measurements.[57] The size-selectivity is related to the ability of a gas molecules to pass through tight constriction points between free volume elements formed by the polymer packing.

Figure 8 shows the diffusion coefficient of O_2, CO_2, N_2, and CH_4 for all four samples of PIM-DTFM-BTrip with different histories. It is possible to construct a data cloud, highlighting the

general trend of decreasing diffusion coefficients with increasing Young's modulus. The solubility coefficient is independent of Young's modulus (Figure S10a), whereas the trend in the permeability (Figure S10b) is a replica of that of the diffusion coefficient, showing that the physical aging has its main impact on diffusion.

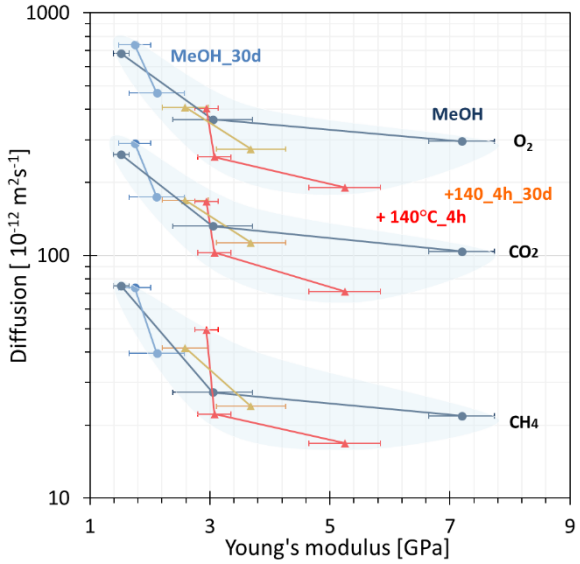

Figure 8. Master plot of the diffusion coefficients of O_2, CH_4 and CO_2 as a function of Young's modulus for all PIM-DTFM-BTrip (**3**) samples with different histories (see sample codes in Table 1). The lines connect the same samples with different ages.

The permeabilities of PIM-1 from Figure 2 would fall below the trend of the ultrapermeable polymers with comparable Young's modulus in Figure S10b. Comparison of PIM-1 with recent data[59] of structurally different and partially fluorinated PIM-2 reveals that PIM-2 has a higher Young's modulus, and although its permeability vs. modulus falls on the PIM-1 trend for CO_2 and O_2, its permeability is substantially higher for CH_4 and N_2 (Figure S11). This suggests that the correlation between Young's modulus and the transport properties only accurate for structurally

similar polymers with similar chain rigidity. Thus, the trend holds for the present family of ultrapermeable polymers with closely related structures. Of course, increased film rigidity is not the only reason for the decreasing permeability and increasing size-selectivity, but it may be expected that free volume also decreased in these samples upon aging. This is a well-known phenomenon for PIMs and has been demonstrated in various studies on PIMs and PIM copolymers.[20,27,60] Free volume is univocally correlated with the transport properties of dense polymers, and both permeability and diffusivity decrease as the FFV decreases.[61]

4 Conclusions

Permeation tests and AFM force spectroscopy studies on a series of different PIM membranes revealed a strong correlation between the transport parameters and the polymer film stiffness. Structurally similar samples with different history follow a nearly universal trend, independent of the specific sample. Excellent agreement between Young's modulus obtained for reference sample PIM-1, and values reported in the literature based on different analytical techniques, show that AFM force spectroscopy offers a practical and convenient alternative to measure the mechanical properties of PIMs. This technique is particularly useful for 'exotic' polymers for which only small samples are available. For the series of structurally similar ultrapermeable PIMs, it was found that the decrease of the diffusion coefficients during aging is associated with an increase in their Young's modulus. Extensive transport studies on one of the samples, PIM-DTFM-BTrip, after different conditioning steps, highlight that the decrease of permeability in time is mainly due to the reduction of the diffusion coefficient. Thermal treatment accelerates the physical aging of the samples in terms of transport parameters but slightly slows down further ageing. Also, in terms of mechanical properties, after an initial increase in Young's modulus there is a slower further increase with time, apparently because the high temperature stabilizes the sample properties.

Interestingly, it appears that the permeation measurement itself affects with the physical aging of these polymers: membranes immediately tested after MeOH treatment or thermal treatment at 140 °C have a significant faster aging compared to the membranes tested only after additional 30 days of aging at ambient conditions. It will be subject of further studies to investigate whether this is due to more efficient removal of MeOH under vacuum, or whether the vacuum exposition during the permeation tests results in higher aging rates. Overall, it can be concluded that the gas permeability and diffusivity systematically decrease with Young's modulus of this series of ultrapermeable PIMs, in a more or less universal trend, regardless of sample history. Some sample-to-sample differences indicate that the correlation is not perfect, and that other independent factors may play a role, such as differences in pore size distribution and fractional free volume.

Table of contents graphic (TOC):

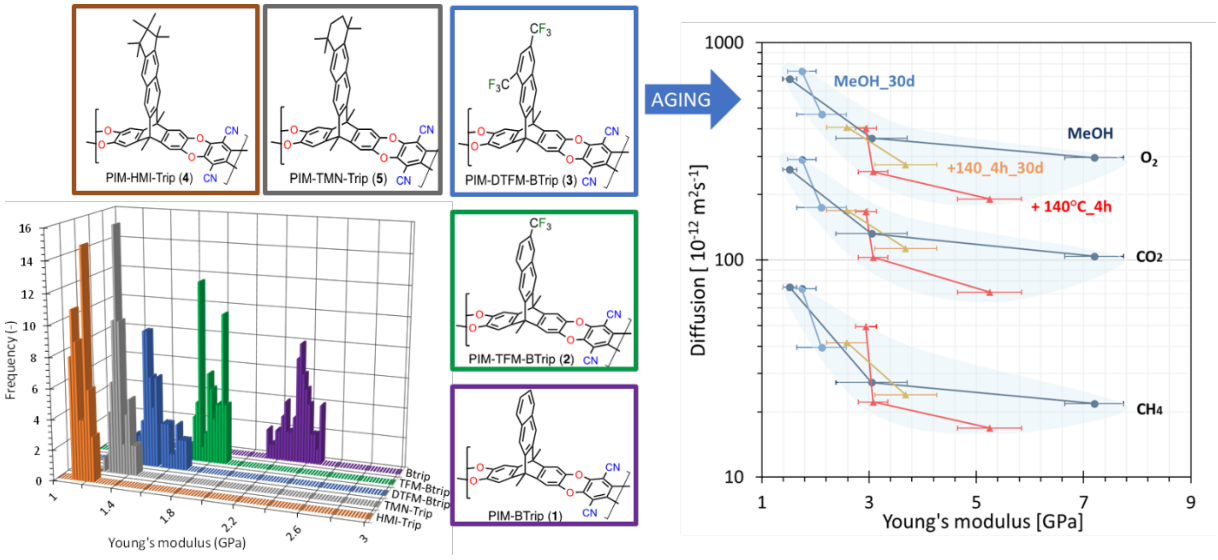

ASSOCIATED CONTENT

Supporting Information.

Figure S1. Correlation of the diffusion and solubility coefficients of O_2, N_2, CH_4 and CO_2 with Young's modulus of PIM-1. Sample after MeOH treatment is represented dark blue and subsequent thermal conditioning at 140 °C under vacuum in red or after 2219 days of aging from the MeOH treatment in light blue. The symbol and the horizontal error bar show the average modulus and the standard deviation of Young's modulus, respectively, calculated from the 60 individual measurements represented in the frequency distributions. The dashed lines are indicated as a guide to the eyes.

Figure S2. SEM images of the cross section of the ultrapermeable PIMs acquired with Phenom Pro X desktop SEM and an acceleration voltage of the primary electron beam of 10 kV in backscattering mode.

Figure S3. Optical micrographs of the membranes surface of ultrapermeable PIMs.

Figure S4. Relative permeability of PIM-DTFM-BTrip (**3**) for O_2, CO_2, N_2 and CH_4 as a function of time in a freshly soaked (black lines) and a thermally treated sample (red lines).

Figure S5. Permeability and diffusion of O_2, N_2, CH_4 and CO_2 of PIM-DTFM-BTrip upon aging of sample MeOH in blue (•), MeOH_30d in light blue (•), +140°C_4h in red (▲), and +140°C_4h_30d in orange (•).

Figure S6. Effect of aging time and thermal treatments on Young's modulus of PIM-DTFM-BTrip MeOH_30d and +140°C_4h_+30d. The two groups in the charts represent the different aging of the samples.

Figure S7. Solubility of H_2, He, O_2, N_2, CH_4 and CO_2 in PIM-DTFM-BTrip as a function of Young's modulus of MeOH in blue (•) and *+140°C_4h* in red (▲).

Figure S8. Correlation between Young's modulus and permeability or diffusion for O_2, N_2, He, H_2, CH_4 and CO_2 for the PIM-DTFM-BTrip samples treated at 140 °C under vacuum for 4 h.

Figure S9. Permeability, diffusion and solubility of O_2, N_2, CH_4, He; H_2 and CO_2 as a function of Young's modulus of PIM-DTFM-BTrip sample MeOH in dark blue (•), MeOH_30d in light blue (•), +140°C_4h in red (▲), and +140°C_4h_30d in orange (▲).

Figure S10. Master plot of permeability and solubility coefficients of O_2, CH_4 and CO_2 as a function of Young's modulus for PIM-DTFM-BTrip samples with different history. The lines connect the same samples with different ages.

Figure S11. Comparison of PIM-1 from Figure 2 with data of fluorinated polymer PIM-2 after the MeOH soaking step (green series),[59] showing reasonable to good correspondence for CO_2 and O_2, but rather strong deviation of CH_4 and N_2 from the trend.

AUTHOR INFORMATION

Corresponding Author

* E-mail: johannescarolus.jansen@cnr.it (J.C.J.)

* E-mail: Neil.McKeown@ed.ac.uk (N.B.M)

ORCID

Mariagiulia Longo: 0000-0002-9407-9148

Maria Penelope De Santo: 0000-0001-6556-3611

Elisa Esposito: 0000-0001-8561-1510

Alessio Fuoco: 0000-0002-8355-0141

Marcello Monteleone: 0000-0001-8339-062X

Lidietta Giorno: 0000-0002-4408-5849

Bibiana Comesaña-Gándara: 0000-0002-6953-6837

C. Grazia Bezzu: 0000-0001-6918-8281

Mariolino Carta: 0000-0003-0718-6971

Johannes C. Jansen: 0000-0003-4538-6851

Neil B. McKeown: 0000-0002-6027-261X

Present Addresses

‖ School of Chemistry, Cardiff University, Cardiff CF10 3AT, U.K. (C.G.B.).

Author Contributions

The manuscript was written through contributions of all authors. All authors have given approval to the final version of the manuscript.

Funding Sources

The work leading to these results has received funding from the European Union's Seventh Framework Program (FP7/2007-2013) under grant agreements n° 608490, project M^4CO_2.

Notes

The authors declare no competing financial interest.

ACKNOWLEDGMENT

Phenom-World B.V., Eindhoven (NL), is gratefully acknowledged for providing a Phenom Pro X desktop SEM for evaluation.

REFERENCES

(1) Sholl, D. S.; Lively, R. P. Seven Chemical Separations to Change the World. *Nature* **2016**, *532* (7600), 435–437.

(2) Galizia, M.; Chi, W. S.; Smith, Z. P.; Merkel, T. C.; Baker, R. W.; Freeman, B. D. 50th Anniversary Perspective: Polymers and Mixed Matrix Membranes for Gas and Vapor Separation: A Review and Prospective Opportunities. *Macromolecules* **2017**, *50* (20), 7809–7843.

(3) Esposito, E.; Dellamuzia, L.; Moretti, U.; Fuoco, A.; Giorno, L.; Jansen, J. C. Simultaneous Production of Biomethane and Food Grade CO 2 from Biogas: An Industrial Case Study. *Energy Environ. Sci.* **2019**, *12* (1), 281–289.

(4) Baker, R. W.; Low, B. T. Gas Separation Membrane Materials: A Perspective. *Macromolecules* **2014**, *47* (20), 6999–7013.

(5) Robeson, L. M. Correlation of Separation Factor versus Permeability for Polymeric

Membranes. *J. Memb. Sci.* **1991**, *62* (2), 165–185.

(6) Robeson, L. M. The Upper Bound Revisited. *J. Memb. Sci.* **2008**, *320* (1–2), 390–400.

(7) Freeman, B. D. Basis of Permeability/Selectivity Tradeoff Relations in Polymeric Gas Separation Membranes. *Macromolecules* **1999**, *32* (2), 375–380.

(8) Budd, P. M.; Ghanem, B. S.; Makhseed, S.; McKeown, N. B.; Msayib, K. J.; Tattershall, C. E. Polymers of Intrinsic Microporosity (PIMs): Robust, Solution-Processable, Organic Nanoporous Materials. *Chem. Commun.* **2004**, *10* (2), 230.

(9) Carta, M.; Malpass-Evans, R.; Croad, M.; Rogan, Y.; Jansen, J. C.; Bernardo, P.; Bazzarelli, F.; McKeown, N. B. An Efficient Polymer Molecular Sieve for Membrane Gas Separations. *Science (80-.).* **2013**, *339* (6117), 303–307.

(10) Ma, C.; Urban, J. J. Polymers of Intrinsic Microporosity (PIMs) Gas Separation Membranes: A Mini Review . *Proc. Nat. Res. Soc.* **2018**, *2* (1), 2002.

(11) Yi, S.; Ghanem, B.; Liu, Y.; Pinnau, I.; Koros, W. J. Ultraselective Glassy Polymer Membranes with Unprecedented Performance for Energy-Efficient Sour Gas Separation. *Sci. Adv.* **2019**, *5* (5), eaaw5459.

(12) Lau, C. H.; Nguyen, P. T.; Hill, M. R.; Thornton, A. W.; Konstas, K.; Doherty, C. M.; Mulder, R. J.; Bourgeois, L.; Liu, A. C. Y.; Sprouster, D. J.; et al. Ending Aging in Super Glassy Polymer Membranes. *Angew. Chemie - Int. Ed.* **2014**, *53* (21), 5322–5326.

(13) Low, Z.-X.; Budd, P. M.; McKeown, N. B.; Patterson, D. A. Gas Permeation Properties, Physical Aging, and Its Mitigation in High Free Volume Glassy Polymers. *Chem. Rev.* **2018**, *118* (12), 5871–5911.

(14) Budd, P. M.; McKeown, N. B.; Ghanem, B. S.; Msayib, K. J.; Fritsch, D.; Starannikova, L.; Belov, N.; Sanfirova, O.; Yampolskii, Y.; Shantarovich, V. Gas Permeation Parameters and Other Physicochemical Properties of a Polymer of Intrinsic Microporosity: Polybenzodioxane PIM-1. *J. Memb. Sci.* **2008**, *325* (2), 851–860.

(15) Lee, M.; Bezzu, C. G.; Carta, M.; Bernardo, P.; Clarizia, G.; Jansen, J. C.; McKeown, N. B. Enhancing the Gas Permeability of Tröger's Base Derived Polyimides of Intrinsic Microporosity. *Macromolecules* **2016**, *49* (11), 4147–4154.

(16) Gemeda, A. E.; De Angelis, M. G.; Du, N.; Li, N.; Guiver, M. D.; Sarti, G. C. Mixed Gas Sorption in Glassy Polymeric Membranes. III. CO2/CH4 Mixtures in a Polymer of Intrinsic Microporosity (PIM-1): Effect of Temperature. *J. Memb. Sci.* **2017**, *524*, 746–757.

(17) Swaidan, R.; Ghanem, B.; Litwiller, E.; Pinnau, I. Physical Aging, Plasticization and Their Effects on Gas Permeation in "Rigid" Polymers of Intrinsic Microporosity. *Macromolecules* **2015**, *48* (18), 6553–6561.

(18) Bernardo, P.; Bazzarelli, F.; Tasselli, F.; Clarizia, G.; Mason, C. R.; Maynard-Atem, L.; Budd, P. M.; Lanč, M.; Pilnáček, K.; Vopička, O.; et al. Effect of Physical Aging on the Gas Transport and Sorption in PIM-1 Membranes. *Polymer (Guildf).* **2017**, *113*, 283–294.

(19) Pilnáček, K.; Vopička, O.; Lanč, M.; Dendisová, M.; Zgažar, M.; Budd, P. M.; Carta, M.; Malpass-Evans, R.; McKeown, N. B.; Friess, K. Aging of Polymers of Intrinsic Microporosity Tracked by Methanol Vapour Permeation. *J. Memb. Sci.* **2016**, *520*, 895–906.

(20) Emmler, T.; Heinrich, K.; Fritsch, D.; Budd, P. M.; Chaukura, N.; Ehlers, D.; Rätzke, K.;

Faupel, F. Free Volume Investigation of Polymers of Intrinsic Microporosity (PIMs): PIM-1 and PIM1 Copolymers Incorporating Ethanoanthracene Units. *Macromolecules* **2010**, *43* (14), 6075–6084.

(21) Mason, C. R.; Maynard-Atem, L.; Al-Harbi, N. M.; Budd, P. M.; Bernardo, P.; Bazzarelli, F.; Clarizia, G.; Jansen, J. C. Polymer of Intrinsic Microporosity Incorporating Thioamide Functionality: Preparation and Gas Transport Properties. *Macromolecules* **2011**, *44* (16), 6471–6479.

(22) Ma, X.; Abdulhamid, M. A.; Pinnau, I. Design and Synthesis of Polyimides Based on Carbocyclic Pseudo-Tröger's Base-Derived Dianhydrides for Membrane Gas Separation Applications. *Macromolecules* **2017**, *50* (15), 5850–5857.

(23) Jue, M. L.; Breedveld, V.; Lively, R. P. Defect-Free PIM-1 Hollow Fiber Membranes. *J. Memb. Sci.* **2017**, *530*, 33–41.

(24) Huang, Y.; Paul, D. R. Physical Aging of Thin Glassy Polymer Films Monitored by Gas Permeability. *Polymer (Guildf).* **2004**, *45* (25), 8377–8393.

(25) Tiwari, R. R.; Jin, J.; Freeman, B. D.; Paul, D. R. Physical Aging, CO2 Sorption and Plasticization in Thin Films of Polymer with Intrinsic Microporosity (PIM-1). *J. Memb. Sci.* **2017**, *537*, 362–371.

(26) Huang, Y.; Paul, D. R. Effect of Film Thickness on the Gas-Permeation Characteristics of Glassy Polymer Membranes. *Ind. Eng. Chem. Res.* **2007**, *46* (8), 2342–2347.

(27) Harms, S.; Rätzke, K.; Faupel, F.; Chaukura, N.; Budd, P. M.; Egger, W.; Ravelli, L. Aging and Free Volume in a Polymer of Intrinsic Microporosity (PIM-1). *J. Adhes.* **2012**, *88* (7),

608–619.

(28) Rowe, B. W.; Freeman, B. D.; Paul, D. R. Physical Aging of Ultrathin Glassy Polymer Films Tracked by Gas Permeability. *Polymer (Guildf).* **2009**, *50* (23), 5565–5575.

(29) Rose, I.; Carta, M.; Malpass-Evans, R.; Ferrari, M.-C.; Bernardo, P.; Clarizia, G.; Jansen, J. C.; McKeown, N. B. Highly Permeable Benzotriptycene-Based Polymer of Intrinsic Microporosity. *ACS Macro Lett.* **2015**, *4* (9), 912–915.

(30) Gorgojo, P.; Karan, S.; Wong, H. C.; Jimenez-Solomon, M. F.; Cabral, J. T.; Livingston, A. G. Ultrathin Polymer Films with Intrinsic Microporosity: Anomalous Solvent Permeation and High Flux Membranes. *Adv. Funct. Mater.* **2014**, *24* (30), 4729–4737.

(31) Tocci, E.; De Lorenzo, L.; Bernardo, P.; Clarizia, G.; Bazzarelli, F.; Mckeown, N. B.; Carta, M.; Malpass-Evans, R.; Friess, K.; Pilnáček, K.; et al. Molecular Modeling and Gas Permeation Properties of a Polymer of Intrinsic Microporosity Composed of Ethanoanthracene and Tröger's Base Units. *Macromolecules* **2014**, *47* (22), 7900–7916.

(32) Polak-Kraśna, K.; Dawson, R.; Holyfield, L. T.; Bowen, C. R.; Burrows, A. D.; Mays, T. J. Mechanical Characterisation of Polymer of Intrinsic Microporosity PIM-1 for Hydrogen Storage Applications. *J. Mater. Sci.* **2017**, *52* (7), 3862–3875.

(33) Polak-Kraśna, K.; Fuhrhop, C.; Rochat, S.; Burrows, A. D.; Georgiadis, A.; Bowen, C. R.; Mays, T. J. AFM Imaging and Nanoindentation of Polymer of Intrinsic Microporosity PIM-1. *Int. J. Hydrogen Energy* **2017**, *42* (37), 23915–23919.

(34) Ma, X.; Pinnau, I. Effect of Film Thickness and Physical Aging on Intrinsic Gas Permeation Properties of Microporous Ethanoanthracene-Based Polyimides. *Macromolecules* **2018**, *51*

(3), 1069–1076.

(35) Song, Q.; Cao, S.; Pritchard, R. H.; Ghalei, B.; Al-Muhtaseb, S. A.; Terentjev, E. M.; Cheetham, A. K.; Sivaniah, E. Controlled Thermal Oxidative Crosslinking of Polymers of Intrinsic Microporosity towards Tunable Molecular Sieve Membranes. *Nat. Commun.* **2014**, *5*.

(36) Budd, P. M.; Elabas, E. S.; Ghanem, B. S.; Makhseed, S.; McKeown, N. B.; Msayib, K. J.; Tattershall, C. E.; Wang, D. Solution-Processed, Organophilic Membrane Derived from a Polymer of Intrinsic Microporosity. *Adv. Mater.* **2004**, *16* (5), 456–459.

(37) Cappella, B.; Dietler, G. Force-Distance Curves by Atomic Force Microscopy. *Surf. Sci. Rep.* **1999**, *34* (1–3), 1–3.

(38) Butt, H. J.; Cappella, B.; Kappl, M. Force Measurements with the Atomic Force Microscope: Technique, Interpretation and Applications. *Surf. Sci. Rep.* **2005**, *59* (1–6), 1–152.

(39) Longo, M.; De Santo, M. P.; Esposito, E.; Fuoco, A.; Monteleone, M.; Giorno, L.; Jansen, J. C. Force Spectroscopy Determination of Young's Modulus in Mixed Matrix Membranes. *Polymer (Guildf).* **2018**, *156*, 22–29.

(40) Yang, G.; Rao, N.; Yin, Z.; Zhu, D. M. Probing the Viscoelastic Response of Glassy Polymer Films Using Atomic Force Microscopy. *J. Colloid Interface Sci.* **2006**, *297* (1), 104–111.

(41) Comesaña-Gándara, B.; Chen, J.; Bezzu, C. G.; Carta, M.; Rose, I.; Ferrari, M.-C.; Esposito, E.; Fuoco, A.; Jansen, J. C.; McKeown, N. B. Redefining the Robeson Upper Bounds for

CO2/CH4 and CO2/N2 Separations Using a Series of Ultrapermeable Benzotriptycene-Based Polymers of Intrinsic Microporosity. *Energy Environ. Sci.* **2019**, *12* (9), 2733–2740.

(42) Hill, A. J.; Pas, S. J.; Bastow, T. J.; Burgar, M. I.; Nagai, K.; Toy, L. G.; Freeman, B. D. Influence of Methanol Conditioning and Physical Aging on Carbon Spin-Lattice Relaxation Times of Poly(1-Trimethylsilyl-1-Propyne). *J. Memb. Sci.* **2004**, *243* (1–2), 37–44.

(43) Seong, J. G.; Zhuang, Y.; Kim, S.; Do, Y. S.; Lee, W. H.; Guiver, M. D.; Lee, Y. M. Effect of Methanol Treatment on Gas Sorption and Transport Behavior of Intrinsically Microporous Polyimide Membranes Incorporating Tröger's Base. *J. Memb. Sci.* **2015**, *480*, 104–114.

(44) Bruker AFM Probes: Force Calibration Cantilevers, Support Note 013-000-000; pp 1–6.

(45) Chizhik, S. A.; Huang, Z.; Gorbunov, V. V.; Myshkin, N. K.; Tsukruk, V. V. Micromechanical Properties of Elastic Polymeric Materials As Probed by Scanning Force Microscopy. *Langmuir* **1998**, *14* (10), 2606–2609.

(46) Weisenhorn, A. L.; Khorsandi, M.; Kasas, S.; Gotzos, V.; Butt, H. J. Deformation and Height Anomaly of Soft Surfaces Studied with an AFM. *Nanotechnology* **1993**, *4* (2), 106–113.

(47) H. Hertz. Ueber Die Berührung Fester Elastischer Körper. *J. für die reine und Angew. Math.* **1882**, *92*, 156–171.

(48) Greaves, G. N.; Greer, A. L.; Lakes, R. S.; Rouxel, T. Poisson's Ratio and Modern Materials. *Nature Materials*. 2011, pp 823–837.

(49) Rose, I.; Bezzu, C. G.; Carta, M.; Comesaña-Gándara, B.; Lasseuguette, E.; Ferrari, M. C.;

Bernardo, P.; Clarizia, G.; Fuoco, A.; Jansen, J. C.; et al. Polymer Ultrapermeability from the Inefficient Packing of 2D Chains. *Nat. Mater.* **2017**, *16* (9), 932–937.

(50) Fraga, S. C.; Monteleone, M.; Lanč, M.; Esposito, E.; Fuoco, A.; Giorno, L.; Pilnáček, K.; Friess, K.; Carta, M.; McKeown, N. B.; et al. A Novel Time Lag Method for the Analysis of Mixed Gas Diffusion in Polymeric Membranes by On-Line Mass Spectrometry: Method Development and Validation. *J. Memb. Sci.* **2018**, *561*, 39–58.

(51) Bernardo, P.; Jansen, J. C.; Bazzarelli, F.; Tasselli, F.; Fuoco, A.; Friess, K.; Izák, P.; Jarmarová, V.; Kačírková, M.; Clarizia, G. Gas Transport Properties of Pebax®/Room Temperature Ionic Liquid Gel Membranes. *Sep. Purif. Technol.* **2012**, *97*, 73–82.

(52) Rochat, S.; Polak-Kraśna, K.; Tian, M.; Mays, T. J.; Bowen, C. R.; Burrows, A. D. Assessment of the Long-Term Stability of the Polymer of Intrinsic Microporosity PIM-1 for Hydrogen Storage Applications. *Int. J. Hydrogen Energy* **2019**, *44* (1), 332–337.

(53) Alberto, M.; Bhavsar, R.; Luque-Alled, J. M.; Vijayaraghavan, A.; Budd, P. M.; Gorgojo, P. Impeded Physical Aging in PIM-1 Membranes Containing Graphene-like Fillers. *J. Memb. Sci.* **2018**, *563*, 513–520.

(54) Park, H. B.; Jung, C. H.; Lee, Y. M.; Hill, A. J.; Pas, S. J.; Mudie, S. T.; Van Wagner, E.; Freeman, B. D.; Cookson, D. J. Polymers with Cavities Tuned for Fast Selective Transport of Small Molecules and Ions. *Science* **2007**, *318* (5848), 254–258.

(55) Fuoco, A.; Rizzuto, C.; Tocci, E.; Monteleone, M.; Esposito, E.; Budd, P. M.; Carta, M.; Comesaña-Gándara, B.; McKeown, N. B.; Jansen, J. C. The Origin of Size-Selective Gas Transport through Polymers of Intrinsic Microporosity. *J. Mater. Chem. A* **2019**, *7* (35),

20121–20126.

(56) Teplyakov, V.; Meares, P. Correlation Aspects of the Selective Gas Permeabilities of Polymeric Materials and Membranes. *Gas Sep. Purif.* **1990**, *4* (2), 66–74.

(57) Fuoco, A.; Comesaña-Gándara, B.; Longo, M.; Esposito, E.; Monteleone, M.; Rose, I.; Bezzu, C. G.; Carta, M.; McKeown, N. B.; Jansen, J. C. Temperature Dependence of Gas Permeation and Diffusion in Triptycene-Based Ultrapermeable Polymers of Intrinsic Microporosity. *ACS Appl. Mater. Interfaces* **2018**, *10* (42), 36475–36482.

(58) Rowe, B. W.; Pas, S. J.; Hill, A. J.; Suzuki, R.; Freeman, B. D.; Paul, D. R. A Variable Energy Positron Annihilation Lifetime Spectroscopy Study of Physical Aging in Thin Glassy Polymer Films. *Polymer (Guildf).* **2009**, *50* (25), 6149–6156.

(59) Fuoco, A.; Satilmis, B.; Uyar, T.; Monteleone, M.; Esposito, E.; Muzzi, C.; Tocci, E.; Longo, M.; De Santo, M. P.; Lanč, M.; et al. Comparison of Pure and Mixed Gas Permeation of the Highly Fluorinated Polymer of Intrinsic Microporosity PIM-2 under Dry and Humid Conditions: Experiment and Modelling. *J. Memb. Sci.* **2020**, *594*, 117460.

(60) Koschine, T.; Rätzke, K.; Faupel, F.; Khan, M. M.; Emmler, T.; Filiz, V.; Abetz, V.; Ravelli, L.; Egger, W. Correlation of Gas Permeation and Free Volume in New and Used High Free Volume Thin Film Composite Membranes. *J. Polym. Sci. Part B Polym. Phys.* **2015**, *53* (3), 213–217.

(61) Yampolskii, Y.; Pinnau, I.; Freeman, B. D. *Materials Science of Membranes for Gas and Vapor Separation*; Yampolskii, Y., Pinnau, I., Freeman, B., Eds.; John Wiley & Sons, Ltd: Chichester, UK, 2006.

(62) Friess, K.; Jansen, J. C.; Vopička, O.; Randová, A.; Hynek, V.; Šípek, M.; Bartovská, L.; Izák, P.; Dingemans, M.; Dewulf, J.; et al. Comparative Study of Sorption and Permeation Techniques for the Determination of Heptane and Toluene Transport in Polyethylene Membranes. *J. Memb. Sci.* **2009**, *338* (1–2), 161–174.

Supporting Information

Correlating gas permeability and rigidity during the physical aging of polymers of intrinsic microporosity using atomic force microscopy

Mariagiulia Longo[†], Maria Penelope De Santo[‡], Elisa Esposito[†], Alessio Fuoco[†], Marcello Monteleone[†], Lidietta Giorno[†], Bibiana Comesaña-Gándara[§], Jie Chen[§], C. Grazia Bezzu[§,//], Mariolino Carta[#], Ian Rose[§], Johannes C. Jansen[†,], Neil B. McKeown[§,*]*

[†] Institute on Membrane Technology, ITM-CNR. Via P. Bucci 17/C, 87036 Rende (CS), Italy.

[‡] Department of Physics and CNR-Nanotec, University of Calabria, Rende (CS), Italy.

[§] EaStCHEM, School of Chemistry, University of Edinburgh, David Brewster Road, Edinburgh, EH9 3FJ, (UK).

[#] Department of Chemistry, Swansea University, College of Science, Grove Building, Singleton Park, Swansea, SA2 8PP, (UK).

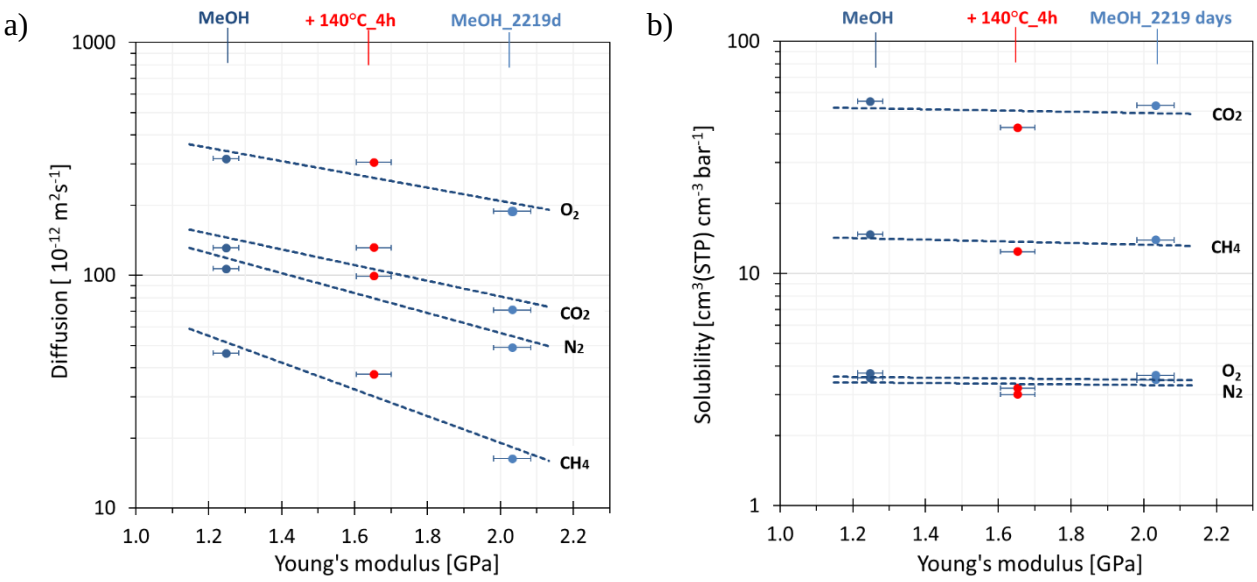

Figure S1. Correlation of the diffusion and solubility coefficients of O_2, N_2, CH_4 and CO_2 with Young's modulus of PIM-1. Sample after MeOH treatment is represented dark blue and subsequent thermal conditioning at 140 °C under vacuum in red or after 2219 days of aging from the MeOH treatment in light blue. The symbol and the horizontal error bar show the average modulus and the standard deviation of Young's modulus, respectively, calculated from the 60 individual measurements represented in the frequency distributions. The dashed lines are indicated as a guide to the eyes.

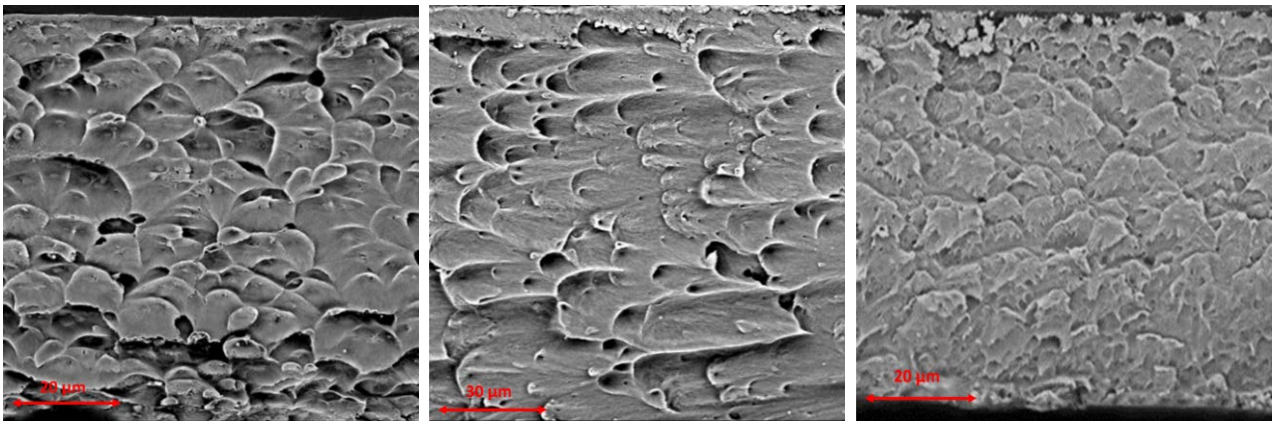

PIM-BTrip **PIM-TFM-BTrip** **PIM-DTFM-BTrip**

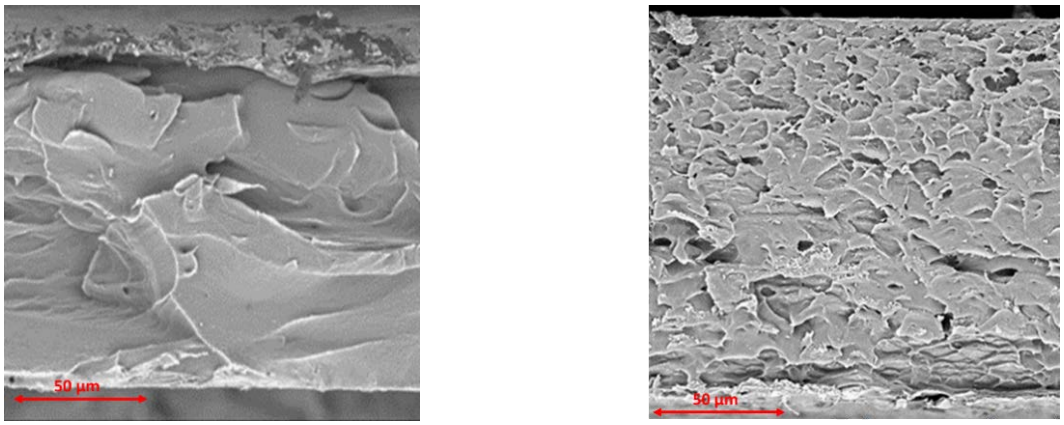

PIM-HMI-Trip **PIM-TMN-Trip**

Figure S2. SEM images of the cross section of the ultrapermeable PIMs acquired with Phenom Pro X desktop SEM and an acceleration voltage of the primary electron beam of 10 kV in backscattering mode.

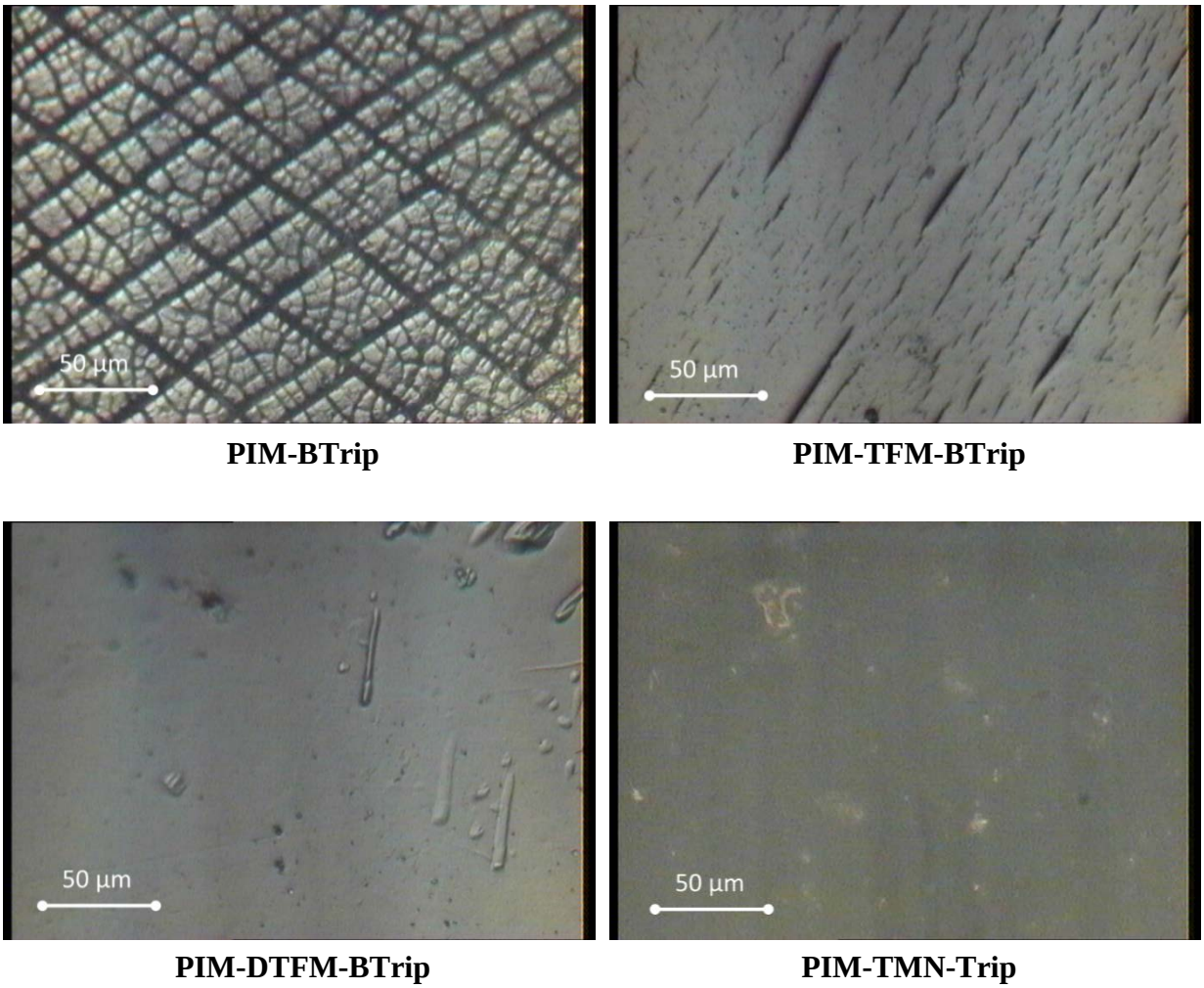

PIM-BTrip **PIM-TFM-BTrip**

PIM-DTFM-BTrip **PIM-TMN-Trip**

Figure S3. Optical micrographs of the membranes surface of ultrapermeable PIMs.

The soaking in methanol PIMs caused a dilation of network and a consecutive evaporation and contraction. The evaporation of MeOH, faster on the surface, induced the visible cracks in PIM-BTrip.[62]

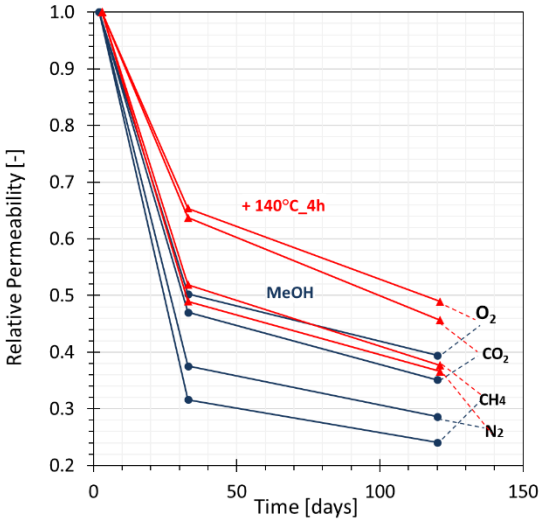

Figure S4. Relative permeability of PIM-DTFM-BTrip (**3**) for O_2, CO_2, N_2 and CH_4 as a function of time in a freshly soaked (black lines) and a thermally treated sample (red lines). Original data from Figure 4a

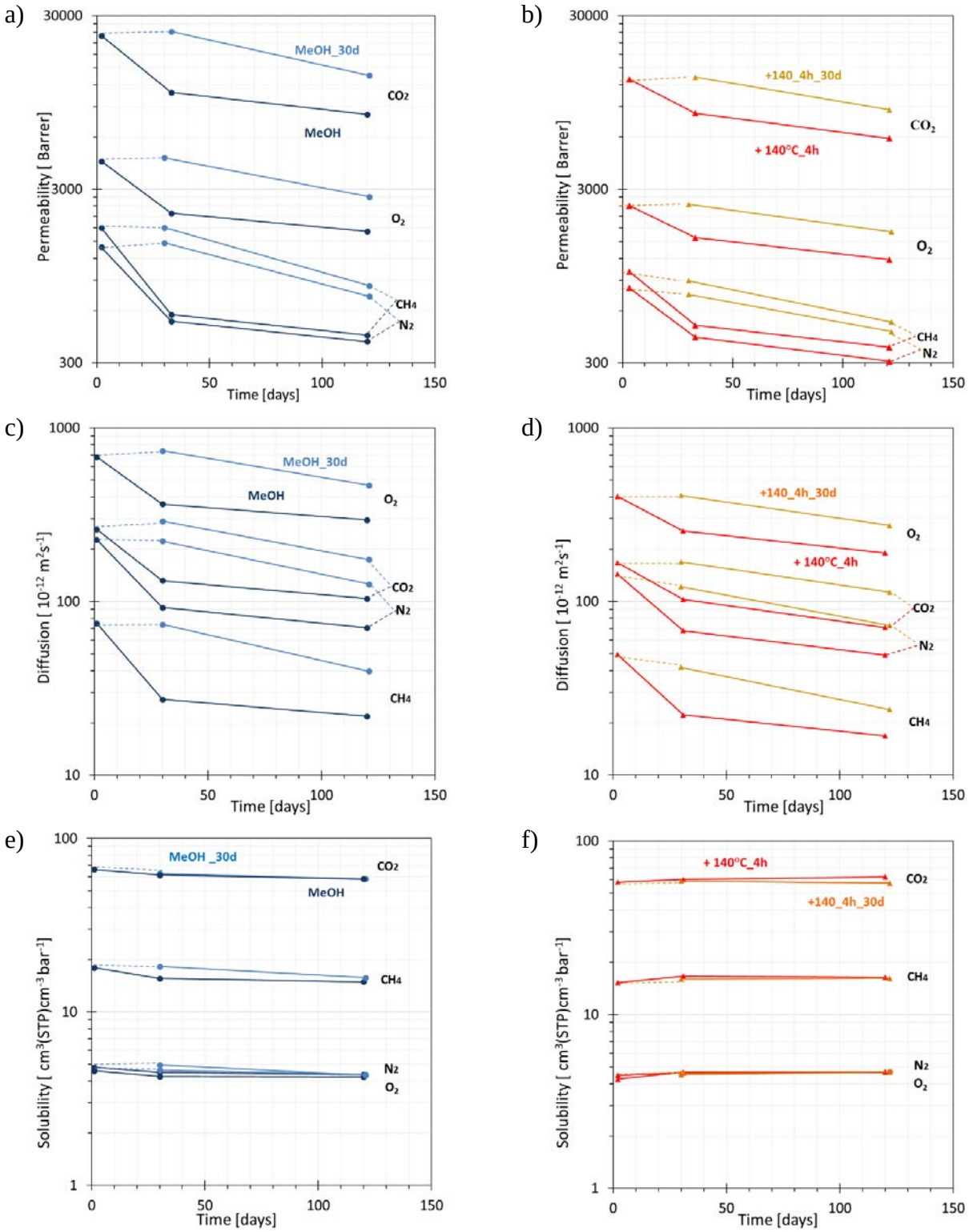

Figure S5. Permeability and diffusion of O_2, N_2, CH_4 and CO_2 of PIM-DTFM-BTrip upon aging of sample MeOH in blue (•), MeOH_30d in light blue (•), +140°C_4h in red (▲), and +140°C_4h_30d in orange (•).

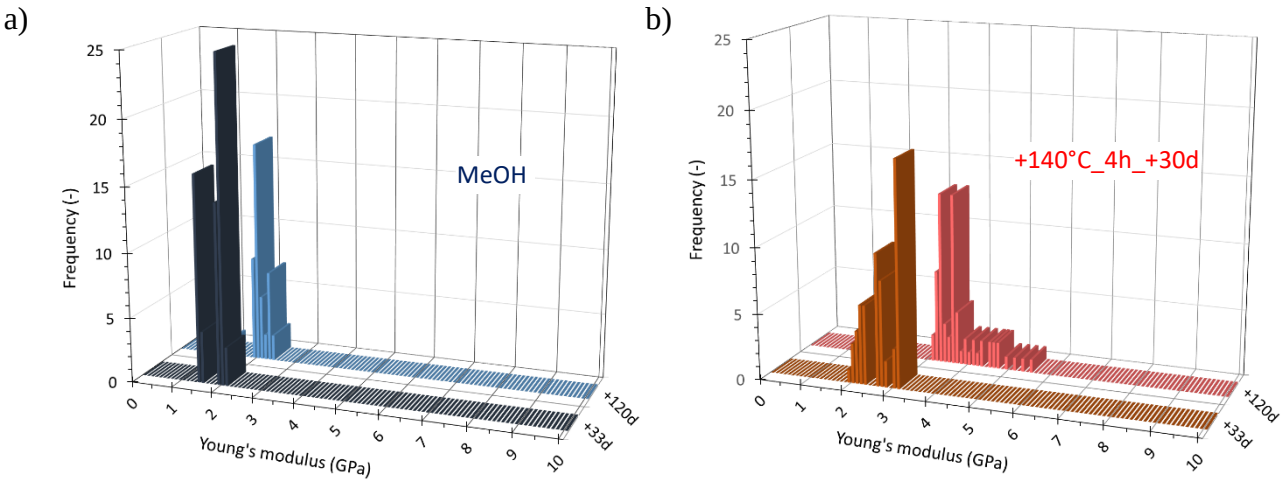

Figure S6. Effect of aging time and thermal treatments on Young's modulus of PIM-DTFM-BTrip MeOH_30d and +140°C_4h_+30d. The two groups in the charts represent the different aging of the samples.

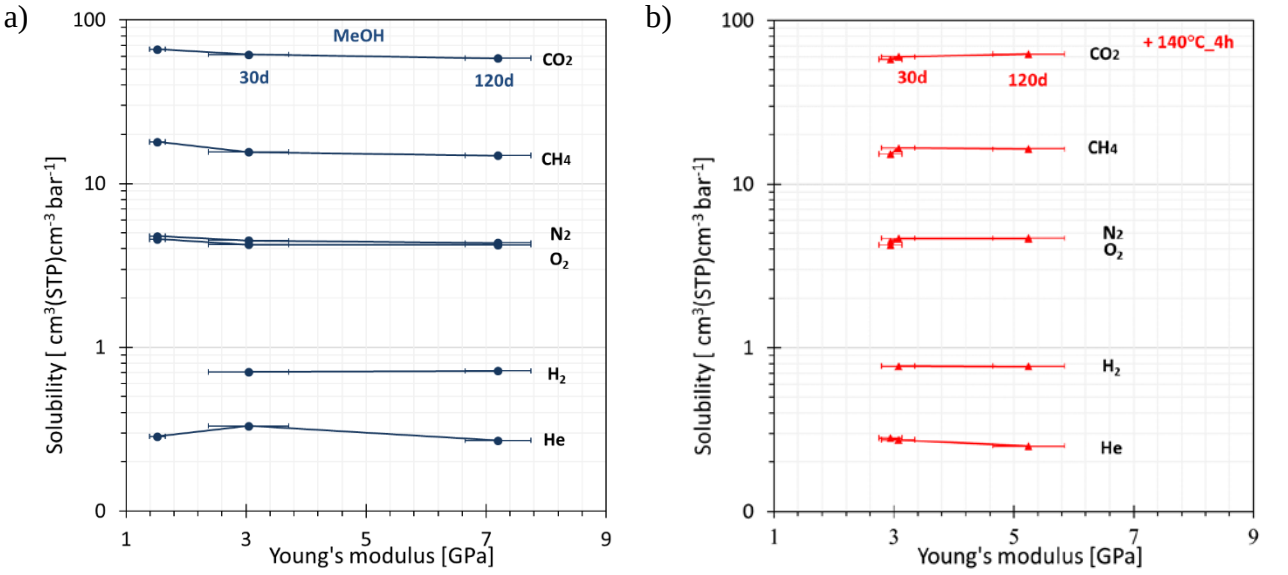

Figure S7. Solubility of H_2, He, O_2, N_2, CH_4 and CO_2 in PIM-DTFM-BTrip as a function of Young's modulus of MeOH in blue (•) and *+140°C_4h* in red (▲).

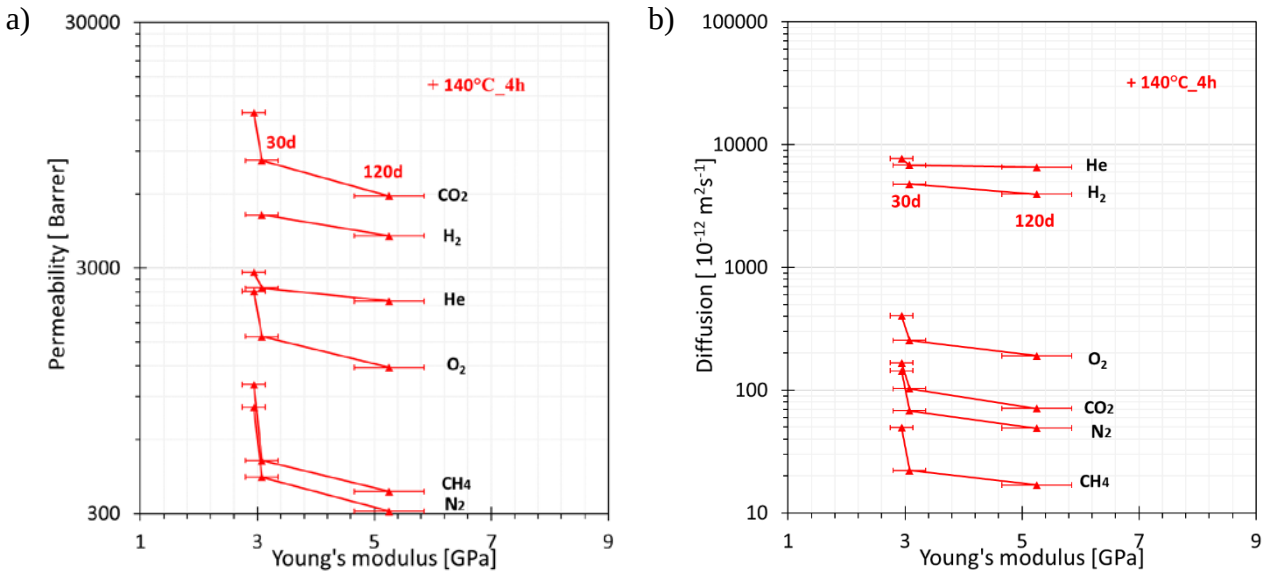

Figure S8. Correlation between Young's modulus and permeability or diffusion for O_2, N_2, He, H_2, CH_4 and CO_2 for the PIM-DTFM-BTrip samples treated at 140 °C under vacuum for 4 h.

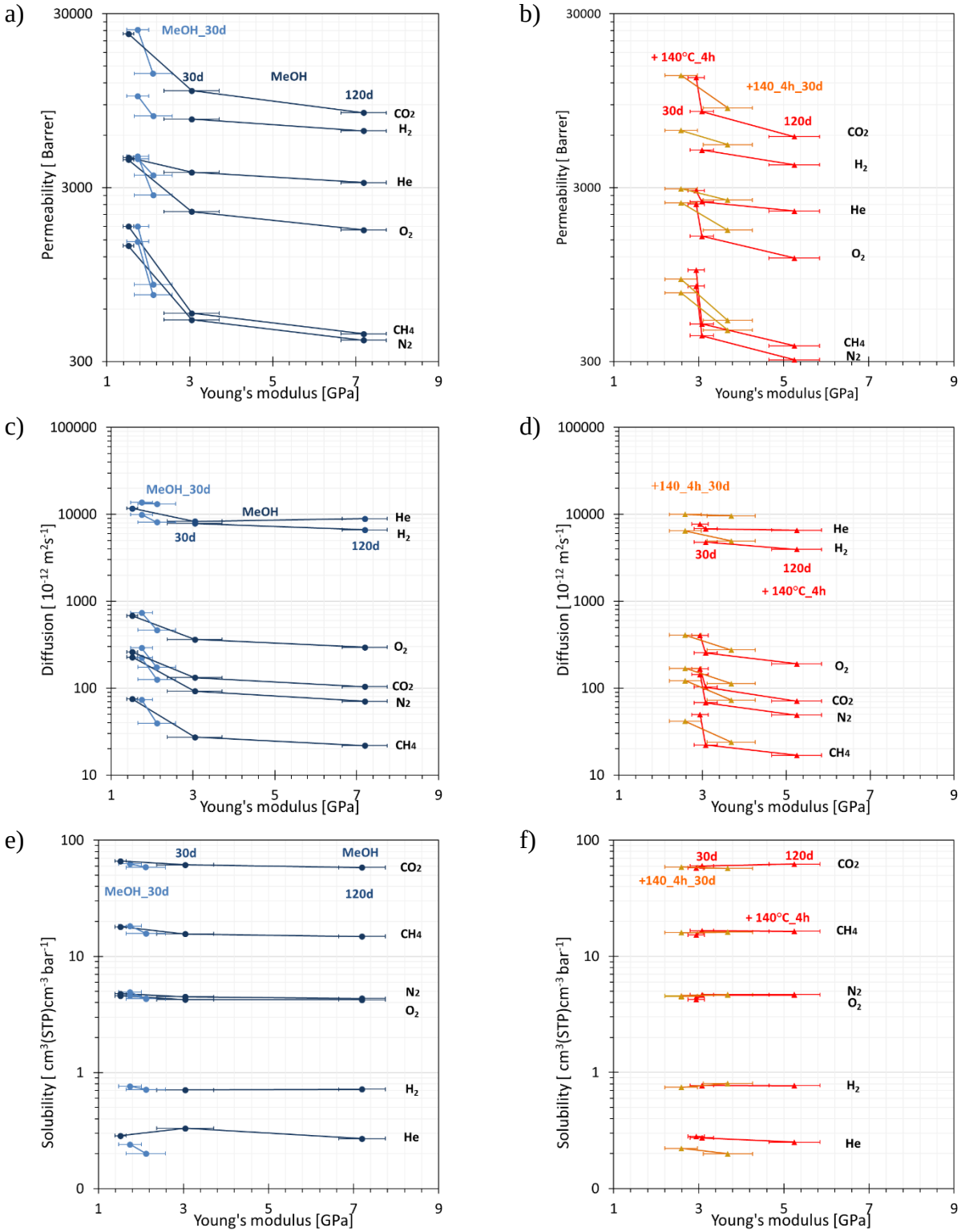

Figure S9. Permeability, diffusion and solubility of O_2, N_2, CH_4, He; H_2 and CO_2 as a function of Young's modulus of PIM-DTFM-BTrip sample MeOH in dark blue (•), MeOH_30d in light blue (•), +140°C_4h in red (▲), and +140°C_4h_30d in orange (▲).

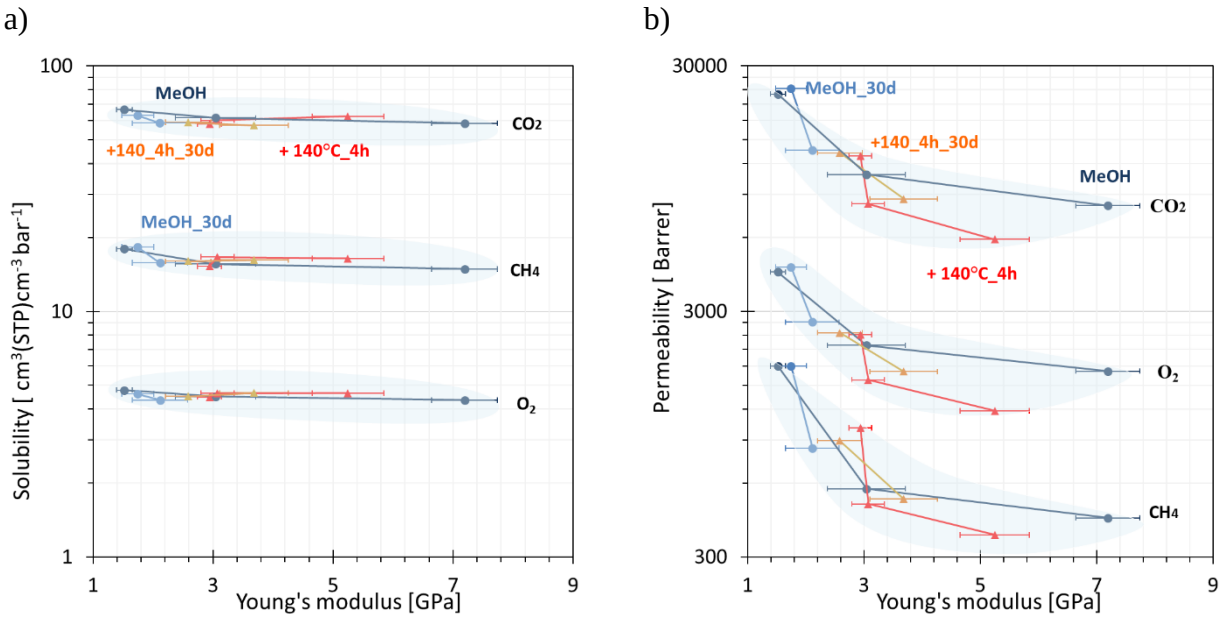

Figure S10. Master plot of permeability and solubility coefficients of O_2, CH_4 and CO_2 as a function of Young's modulus for PIM-DTFM-BTrip samples with different history. The lines connect the same samples with different ages.

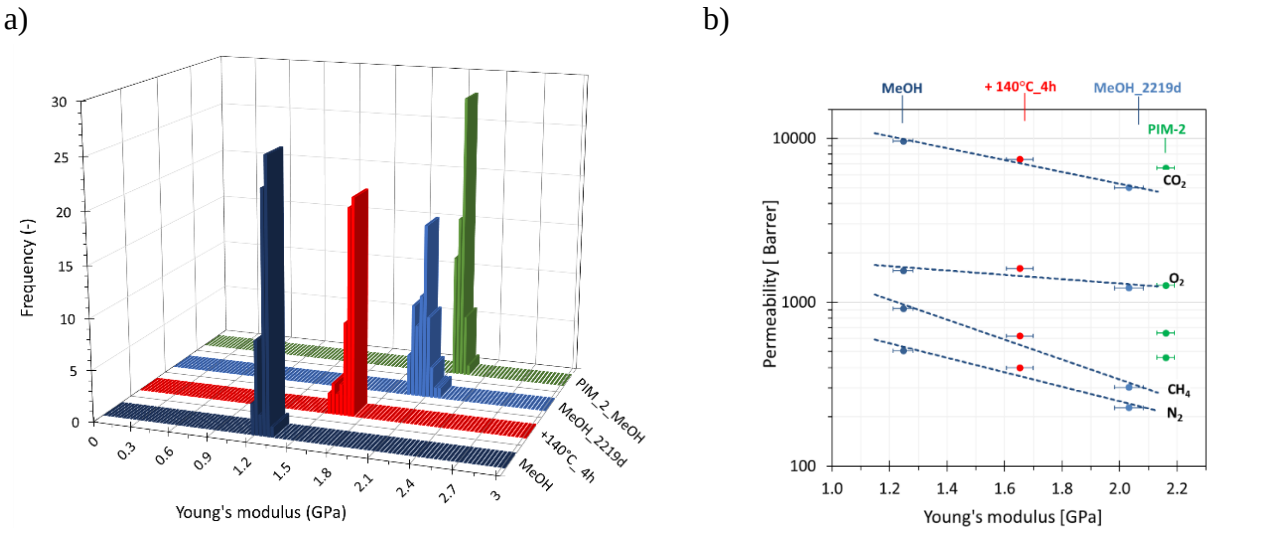

Figure S11. Comparison of PIM-1 from Figure 2 with data of fluorinated polymer PIM-2 after the MeOH soaking step (green series),[59] showing reasonable to good correspondence for CO_2 and O_2, but rather strong deviation of CH_4 and N_2 from the trend.